Vol. 734: 1–21, 2024
https://doi.org/10.3354/meps14567

MARINE ECOLOGY PROGRESS SERIES
Mar Ecol Prog Ser

Published April 18

Changing phytoplankton phenology in the marginal ice zone west of the Antarctic Peninsula

Jessica S. Turner[1,*], Heidi Dierssen[1], Oscar Schofield[2], Heather H. Kim[3], Sharon Stammerjohn[4], David R. Munro[4,5], Maria Kavanaugh[6]

[1]Department of Marine Sciences, University of Connecticut, Groton, CT 06340, USA
[2]Department of Marine and Coastal Sciences, Rutgers University, New Brunswick, NJ 08901, USA
[3]Department of Marine Chemistry and Geochemistry, Woods Hole Oceanographic Institution, Woods Hole, MA 02453, USA
[4]Cooperative Institute for Research in Environmental Sciences, University of Colorado, Boulder, CO 80309, USA
[5]National Oceanic and Atmospheric Administration, Global Monitoring Laboratory, Boulder, CO 80309, USA
[6]College of Earth, Ocean, and Atmospheric Sciences, Oregon State University, Corvallis, OR 97331, USA

ABSTRACT: Climate change is altering global ocean phenology, the timing of annually occurring biological events. We examined the changing phenology of the phytoplankton accumulation season west of the Antarctic Peninsula to show that blooms are shifting later in the season over time in ice-associated waters. The timing of the start date and peak date of the phytoplankton accumulation season occurred later over time from 1997 to 2022 in the marginal ice zone and over the continental shelf. A divergence was seen between offshore waters and ice-associated waters, with offshore bloom timing becoming earlier, yet marginal ice zone and continental shelf bloom timing shifting later. Higher chlorophyll *a* (chl *a*) concentration in the fall season was seen in recent years, especially over the northern continental shelf. Minimal long-term trends in annual chl *a* occurred, likely due to the combination of later start dates in spring and higher chl *a* in fall. Increasing spring wind speed is the most likely mechanism for later spring start dates, leading to deeper wind mixing in a region experiencing sea ice loss. Later phytoplankton bloom timing over the marginal ice zone and continental shelf will have consequences for surface ocean carbon uptake, food web dynamics, and trophic cascades.

KEY WORDS: Phenology · Antarctic ecology · Remote sensing · Marginal ice zone · Chlorophyll *a* · Polar regions · Phytoplankton blooms · Satellite data

1. INTRODUCTION

Phenology involves the timing of annually recurring events in nature. For ocean ecosystems, a prominent annual event is the start date of the phytoplankton accumulation season, commonly referred to as the start of the spring bloom. In this paper, we use the term 'accumulation season' to describe the period during each year when phytoplankton biomass as measured by surface chlorophyll *a* (chl *a*) concentration is increasing, such that the average phytoplankton mass-specific loss rates are smaller than their growth rates. The spring bloom is the foundation of the marine food web. The intense seasonal surge in primary production supports the zooplankton community, which in turn provides a rich food source for fish and other higher trophic level organisms (Riley 1942, Fenchel 1988, Winder & Sommer 2012). As climate warms, most research predicts earlier start dates for the phytoplankton accumulation season in the world's oceans. On average, studies show a shift toward earlier phytoplankton bloom timing by approximately 4 d per decade (Poloczanska et al. 2013, 2016, IPCC 2019). Satellite remote sensing of global phyto-

*Corresponding author: jturner@uconn.edu

Publisher: Inter-Research · www.int-res.com

plankton blooms similarly suggests that the phytoplankton accumulation season is starting earlier and lasting longer (Friedland et al. 2018).

High-latitude polar ecosystems are often treated as a single entity in global studies of phytoplankton phenology characterized by short-duration, high-intensity summer phytoplankton blooms (Racault et al. 2012). Satellite-derived chl *a* in the Southern Ocean reveals increasing trends over time in offshore open ocean waters in most sectors (Del Castillo et al. 2019, Pinkerton et al. 2021). Indeed, the Intergovernmental Panel on Climate Change (IPCC 2019, p. 205) summarizes with 'high confidence' that changes in polar sea ice and ocean stratification are occurring, causing changes in the 'timing, duration, and intensity of primary production.' In a warming climate, start dates of the phytoplankton accumulation season at high latitudes are predicted to shift earlier by about 5 d per decade (Friedland et al. 2018, Henson et al. 2018).

However, polar seas with seasonal sea ice experience more variability than the broad high-latitude regions examined in global phenology modeling studies. The marginal ice zone (MIZ) experiences the highest seasonal variability in sea ice cover for a given polar region (Tréguer & Jacques 1992). In Antarctic waters, the MIZ comprises ~6 million km^2 of about 19 million km^2 of total Antarctic sea ice cover (32%) and makes up a majority of the sea ice cover for the West Antarctic Peninsula (WAP) region (~60%) (Stroeve et al. 2016, Vichi 2022). Sea ice variability in the MIZ is linked to variability in phytoplankton and krill populations; thus, this region plays an important role in supporting the marine ecosystem throughout many trophic levels. The MIZ surrounding Antarctica experiences some of the highest winds and waves on the planet, and it is here where the timing of sea ice retreat and advance, light availability, wind-driven mixing, bathymetric effects on mixing, and nutrient supply are highly variable over both space and time. Changes such as increased wind-driven mixing resulting in reduced stratification early in the season can shift the timing of the start date of the phytoplankton accumulation season later in the year, a scenario which has been observed in other polar seas with seasonal sea ice (Stabeno et al. 2001, 2012).

In this paper, we explore the seasonal phenology of phytoplankton biomass at a sentinel region for polar ecosystem change: the marine system of the WAP (Henley et al. 2019). The WAP is often used as a case study for changing polar systems due to its declining seasonal sea ice, melting of nearby glaciers, exposure to high circumpolar winds, currents, and waves, a dynamic food web, and regionally relevant sinks for anthropogenic CO_2 (Arrigo et al. 2008, Henley et al. 2019). The WAP region is governed by the seasonal presence of sea ice, whose dynamics are driven by multiple climatic forcings (Stammerjohn et al. 2008, Meredith et al. 2017, 2021). High chl *a* concentrations at the surface depend in part on low wind speeds (Saba et al. 2014), as deeper mixing may result in both dilution and light limitation. Each spring season, sea ice melt leads to stratification, which allows for initiation of the phytoplankton accumulation season (Moline 1998, Vernet et al. 2008, Carvalho et al. 2016, Schofield et al. 2018). Later in the summer season, glacial melt can also sustain or intensify coastal stratification, thus supporting or sustaining high phytoplankton biomass in surface waters (Dierssen et al. 2002, Meredith et al. 2021).

Most *in situ* observations in polar systems are collected during the summer, limiting knowledge of seasonal phenology. For example, January *in situ* observations show trends toward shallower summer mixed-layer depths (MLD), increased summer primary production, and enhanced summer carbon drawdown along the WAP (Schofield et al. 2018, Brown et al. 2019). However, phytoplankton dynamics need to be examined throughout the polar season for a better understanding of ecosystem function and carbon cycling. Such phenology analysis allows for the evaluation of climatological changes in polar regions and for predicting impacts on food web dynamics. Previous time series analyses along the WAP with high temporal coverage (Saba et al. 2014, Kim et al. 2018, Brown et al. 2019, Thibodeau et al. 2019, Cimino et al. 2023) are spatially limited to either the sampling grids of research vessels or point locations at coastal research stations. Satellite remote sensing of ocean color provides the means to study phytoplankton dynamics from September to April, with wide spatial coverage and a 25 yr time series (1997 to 2022). Ocean color remote sensing is inherently limited by some factors, such as surface-only chl *a* estimates without depth-integrated biomass, chl *a* as an imperfect proxy for biomass, limited retrievals at high solar zenith angles, clouds, and the need to correct for atmospheric and surface phenomena that interfere with estimates of water-leaving radiance. Despite these limitations, remote sensing is an indispensable tool for ocean observing thanks to increased spatial and temporal coverage in polar regions with limited accessibility. Ocean color remote sensing in western Antarctica is useful for studying phytoplankton rather than other optically-active constituents, since there are no major terrestrial sources of sediments (Pan et al. 2019) or colored dissolved

organic matter (Patterson 2000, Norman et al. 2011). Ocean color data are useful for the WAP region from 1997 onward, beginning with the SeaWiFS sensor (see the Appendix for a list of abbreviations used in this paper). The earlier Coastal Zone Color Scanner (CZCS) (e.g. Montes-Hugo et al. 2009) is not appropriate for long-term analysis of polar regions, since spatial coverage is limited to the northern WAP, limiting synoptic view of feature migration and correlations with the migration of the seasonal sea ice margin (Figs. S1 & S2 in the Supplement at www.int-res.com/articles/suppl/m734p001_supp.pdf).

The objectives of this study were to (1) quantify the time series of satellite-derived surface chl *a* up to recent years, (2) illustrate spatial gradients and temporal trends in chl *a* and its seasonal timing, and (3) identify long-term shifts in the timing of phenological events in the phytoplankton accumulation season along the WAP. Results show that the phytoplankton accumulation season is starting and peaking later over time throughout much of the WAP region, with decreased chl *a* in the spring season and increased chl *a* in the fall season in recent years.

2. METHODS

2.1. Study area

The WAP region (80 to 55° W, 70 to 60° S) was analyzed, including both the offshore and shelf environments. Five ecoregions were used: the Southern Polar Front (SPF), the MIZ, the northern shelf, the mid-shelf, and the southern shelf (Fig. 1). The SPF corresponds to the Permanently Open Ocean Zone, which is considered an almost oligotrophic ocean experiencing light limitation due to high wind mixing and nutrient limitation (Jeandel et al. 1998). The MIZ is influenced by the receding ice edge each spring and advancing ice edge each fall, and this ecoregion is more productive than the Permanently Open Ocean Zone but not as productive as the shelf and coast (Tréguer & Jacques 1992). The shelf, sometimes labeled the Coastal and Continental Shelf Zone, is considered the most productive region of the Southern Ocean, with large blooms occurring over the course of the phytoplankton accumulation season (Arrigo & McClain 1994, Smith et al. 1996, Dierssen et al. 2000). We further divided the shelf into 3 ecoregions from north to south based on the phenology of bloom timing and seasonal sea ice retreat (Fig. 1). Thus, ecoregions correspond to both bathymetric gradients (i.e. shelf vs. off-shelf) and the spatial gradients in the mean timing of bloom start dates. The line between the SPF and the MIZ approximately corresponds to both the northern limit of the sea ice zone and the southern boundary of the Antarctic Circumpolar Current, known as the southern Antarctic Circumpolar Current front (Orsi et al. 1995, Martinson 2012, Chapman et al. 2020).

2.2. Satellite ocean color data

2.2.1. Satellite-derived chl *a*

Satellite-derived chl *a* data were sourced from CMEMS GlobColour (Garnesson et al. 2019). This product is a merged multi-sensor data set using chl *a*

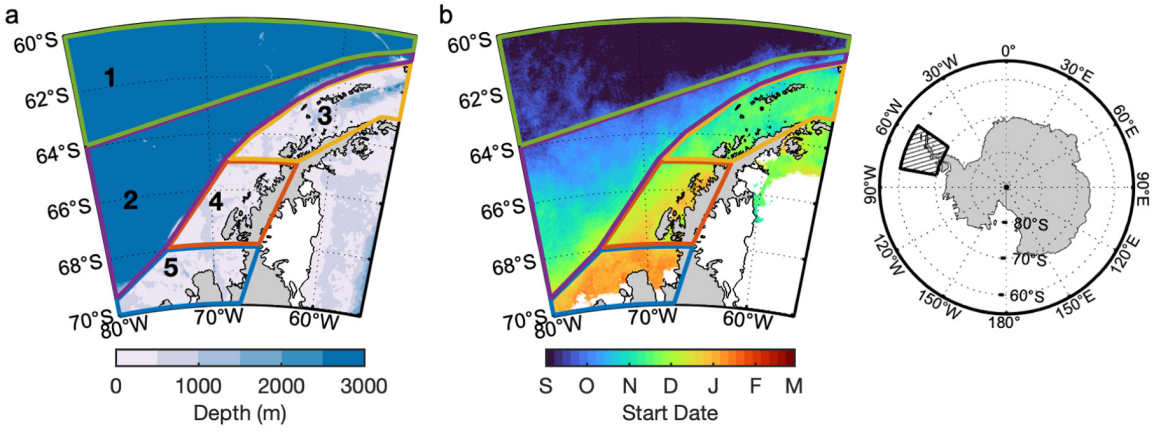

Fig. 1. West Antarctic Peninsula, with regions overlaid on (a) bathymetry and (b) mean start date of the phytoplankton accumulation season 1997–2022. Months indicate the first day of each month (e.g. 'S' = 1 September). Regions include 1: Southern Polar Front, 2: marginal ice zone, 3: northern shelf, 4: mid-shelf, and 5: southern shelf. Gray indicates land, white indicates ice shelves. In (b), non-ice shelf areas that are colored white correspond with satellite data where <30% of daily scenes were present due to frequent presence of sea ice

data from SeaWiFS (1997–2010), MODIS-Terra (2000–present), MODIS-Aqua (2002–present), MERIS (2002–2012), VIIRS-NPP (2012–present), VIIRS-NOAA20 (2018–present), OLCI-S3A (2016–present), and OLCI-S3B (2018–present), processed to a common spatial resolution of 4 km. Chl *a* from this record is a daily interpolated gap-filled Level-4 data product, flagged and processed as in Garnesson et al. (2019). Gap-filled and non-gap-filled chl *a* concentrations were consistent with one another in the WAP region over the time series analyzed in this study (Fig. S3). The chl *a* algorithm in this data set is a global algorithm based on the tendency of phytoplankton to absorb comparatively more blue light relative to green (Gohin et al. 2002, Hu et al. 2012, Garnesson et al. 2019). Merging of data from multiple sensors created some inconsistencies in the time series due to the addition of higher spatial resolution sensors such as MERIS and OLCI in later years (Van Oostende et al. 2022). However, most of those inconsistencies occur in very nearshore waters due to the enhanced ability of the added sensors to observe specific geographical pixels. This data set (Turner 2024) is suitable for our analysis thanks to the broad spatial coverage of the ecoregions in this study, including mostly offshore waters not impacted by the addition of higher spatial resolution sensors.

Global chl *a* algorithms are known to underestimate *in situ* chl *a* in the WAP region by a factor of 2 to 2.5 due to a combination of pigment packaging, low particulate backscattering, and low concentrations of dissolved substances (Mitchell & Holm-Hansen 1991, Mitchell 1992, Dierssen 2000, Dierssen & Smith 2000, Kahru & Mitchell 2010, IOCCG 2015). To correct for the underestimation by global algorithms, we applied a fourth-order polynomial to the global chl *a* data set to match field data (Dierssen and Smith 2000). As shown in Figs. S4 & S5 in the Supplement, this correction is minimal at low chl *a* concentrations representative of offshore waters in the SPF, where the standard algorithms generally perform well (Dierssen 2000, Haëntjens et al. 2017). These corrections are conducted to better reflect the range in chl *a* from shelf to open ocean in the WAP region. Because phenology analysis depends on the relative chl *a* rather than absolute chl *a*, and because the correction is consistent throughout the satellite time series, it does not impact the analyses of chl *a* phenology over time.

The use of satellite-derived surface chl *a* as a tool to study phytoplankton dynamics is useful in polar regions despite some inherent limitations. Chl *a* is an imperfect metric for phytoplankton biomass, since the ratio of chl *a* to biomass can vary with phytoplankton carbon, light, temperature, and nutrient concentrations (Cleveland et al. 1989, Babin et al. 1996, Geider et al. 1997, Barbieux et al. 2018). In some systems, chl *a* in the surface ocean may exhibit different patterns compared to vertically integrated phytoplankton biomass throughout the water column, as seen in the North Atlantic (Boss & Behrenfeld 2010). The relationship between surface and depth-integrated chl *a* is generally well constrained in the WAP region (Dierssen et al. 2000).

2.2.2. Satellite data availability

Satellite data availability enables analysis over austral spring, summer, and early fall for areas that are generally free of sea ice during the summer season in most years (Fig. S6). Available data are deemed accumulation season data since low light and under-sea-ice data are unavailable in austral winter. Data are available for the entire WAP region from September to April, partially unavailable in May and August, and completely unavailable in June and July due to low light and ice cover (Fig. 2; Fig. S7).

2.3. Environmental data

Long-term trends in environmental factors were analyzed in addition to chl *a*, including wind speed, photosynthetically active radiation (PAR), and sea surface temperature (SST). ERA5 reanalysis data were used to analyze trends in wind speed over time (Copernicus Climate Change Service 2018). Hourly wind speeds were calculated from hourly *u*- and *v*-component velocities at 0.25° × 0.25° horizontal resolution at 10 m above Earth's surface using wind speed = sqrt(u^2 + v^2). Hourly wind speeds were averaged to daily and monthly wind speeds. For wind, relevant data assimilated into the ERA5 wind product include satellite observations (infrared and microwave radiances, retrievals from radiance data, and scatterometer data) and *in situ* observations (ships, aircraft, buoys, radar, and radiosondes). Due to the known low quantity of *in situ* data and low reliability of satellite observations of the sea surface in the presence of seasonal sea ice, only ERA5 reanalysis data in the offshore SPF ecoregion were analyzed (Fig. 1). PAR data were downloaded from NASA Ocean Color Web from SeaWiFS, MODIS-Terra, and MODIS-Aqua (Frouin & Pinker 1995, Frouin et al. 2002, 2012) as a Level-3 daily product at 9 km spatial resolution. This data set provides an

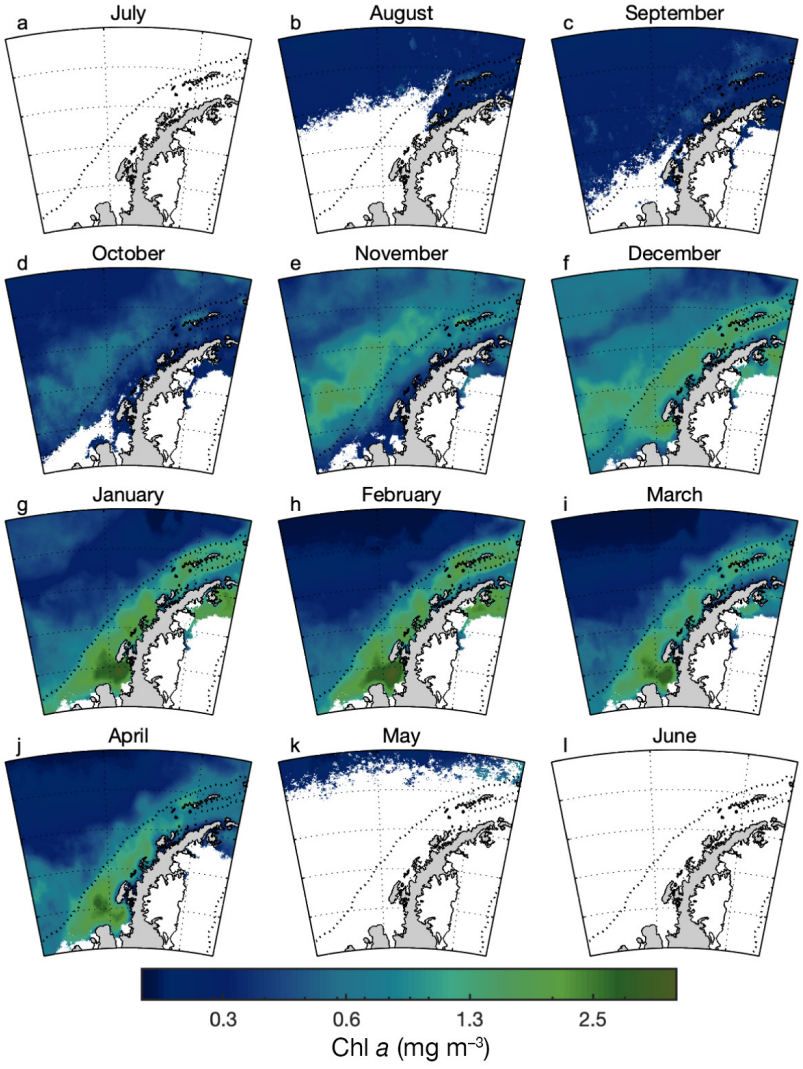

Fig. 2. Monthly climatologies of chlorophyll *a* (chl *a*), showing the average of 1997–2022 for each month. Climatologies were calculated for spatial points where >75% of data were available (>18 of 24 years). White space in some months indicates where satellite data are unavailable due to sea ice and low light. Black dotted line indicates the continental shelf break (1000 m isobath)

estimate of daily average PAR in Einstein m^{-2} d^{-1} based on observed top-of-atmosphere radiances in in the 400–700 nm range that do not saturate over clouds. For years with multiple sensors in orbit at once (i.e. SeaWiFS, MODIS-Terra, and MODIS-Aqua for years 2002–2010), PAR data from all sensors were averaged for each day to create 1 average mapped file per day. Since PAR data from ocean color using this approach are only valid over dark waters and are invalid over sea ice as a result of the plane-parallel algorithm, only PAR data in the offshore SPF ecoregion were analyzed (Fig. 1). SST data were downloaded from the Global Ocean OSTIA Sea Surface Temperature and Sea Ice Reprocessed data set from CMEMS as a Level-4 daily product at 0.05° × 0.05° horizontal resolution (Good et al. 2020).

2.4. Data analysis

2.4.1. Spatial and temporal boundaries of analysis

Spatially, analysis was performed only for ocean color data pixels where at least 30% of daily data were present, which removed noise by excluding locations covered by seasonal sea ice for the majority of the time series (Fig. S6). Temporally, data were analyzed by austral year, 1 July through 30 June, to encompass the entire southern hemisphere accumulation season rather than the boreal calendar year. The data set includes September 1997 through August 2022.

2.4.2. Phenology metrics

Analysis of changing timing of phytoplankton dynamics focused on the start date of the phytoplankton accumulation season, referred to here as the 'start date.' In addition to the start date, we examined the 'peak date,' i.e. the timing of the maximum concentration of chl *a*. While global studies often use bloom duration as a metric of phytoplankton phenology (Racault et al. 2012, 2015, Friedland et al. 2018), the WAP region is unsuitable for the traditional definition of bloom duration. In many parts of the WAP, especially over the shelf, prolonged elevated chl *a* concentrations continue throughout the austral summer and fall (Kim et al. 2018). High chl *a* concentrations, while variable, can persist into the fall season up until low light and sea ice advance render satellite observations unusable. Thus, instead of duration, we focused on start date and peak date as the most suitable metrics. Each of these phenology metrics was calculated for each year in the 25 yr record as day of austral year from 1 July to 30 June. The metrics start date and peak date were therefore truly temporally independent from year to year, representing individual annual values in

units of day of year (DOY). Decadal trends were compared using the austral years (July to June) 2000–2001 through 2010–2011 versus 2011–2012 through 2021–2022. These sets of years were chosen based on change-point analysis for the start date and peak date time series for each region (Killick et al. 2012). Change-point analysis showed distinct change-points in the year 2012 for the MIZ, northern shelf, and mid-shelf ecoregions (Figs. S8 & S9).

2.4.3. Phenology metric sensitivity analysis

There are several different ways of looking at changes in the phenology of phytoplankton blooms (Brody et al. 2013, Thomalla et al. 2015). We tried multiple methods (Fig. S10) and chose the threshold approach, because it showed the clearest spatial gradient in the average timing of the start date across all years and fell in the middle of the distribution of all indices in terms of resulting trends over time (Fig. S10). The threshold approach defines the start of the phytoplankton accumulation season as the day when chl *a* becomes greater than the threshold value equal to the long-term median plus 5% (Siegel et al. 2002, Racault et al. 2012) and remains above that threshold value for 5 consecutive days.

For a given location in the waters west of the Antarctic Peninsula, a typical year begins with low chl *a* when satellite data first become available, then increases to a peak chl *a* value in mid-summer, then decreases with shortening day length and sea ice advance. However, some locations during some years experienced 'no bloom' as defined by never exceeding 2.5 times the long-term threshold value (where the threshold value is the long-term median plus 5%, i.e. 0.4 mg m^{-3} for the mid-shelf). Therefore, additional quality control was performed by removing years without a substantial phytoplankton bloom from all phenology analyses. This quality control measure had only a small effect, since 19 of 25 years experienced a substantial bloom for >90% of the ocean area analyzed, and even the year with the largest number of 'no bloom' locations (1998) showed substantial blooms in 77% of pixels (Fig. S11).

2.5. Statistical analysis

Time series analysis was performed for the WAP region as a whole using mapped long-term trends at each *x*,*y* pixel location and for separate ecoregions. Ecoregion time series were created by averaging the pixels (geometric mean) within the polygons shown in Fig. 1. For all statistical tests, we used a significance threshold of 0.05.

To determine the significance of decadal differences in the daily time series, we applied a Kruskal-Wallis test, i.e. non-parametric ANOVA, 'kruskalwallis' function in MATLAB 9.6.0 R2019a (The MathWorks Inc. 2019) to compare each DOY mean chl *a* for 2001–2011 to the same DOY mean chl *a* for 2012–2022 in each ecoregion. The application of a non-parametric test was appropriate since the distributions of decadal chl *a* by DOY (e.g. chl *a* for 1 December in the northern shelf across all years in a given decade) were non-normal. The null hypothesis is that both decades have the same center parameter for their distribution.

To assess the significance of decadal differences in start date and peak date by ecoregion, we calculated the spatial mean of each metric in each ecoregion during each year to find the decadal means and medians, then compared decadal medians using non-parametric Kruskal-Wallis tests. Like the test above, the null hypothesis is that both decades have the same center parameter for their distribution. The application of a non-parametric test was appropriate since decadal start dates and peak dates by ecoregion (e.g. northern shelf mean start date across all years in a given decade) were not normally distributed.

Mapped long-term trends in each phenology metric and in month-wise chl *a* were calculated using Theil-Sen non-parametric estimates of slope over time (Gilbert 1987) at each *x*,*y* location, using the 'TheilSen' function in MATLAB R2019a (Danziger 2024). The statistical significance of these mapped trends was tested at each *x*,*y* location using a non-parametric Mann-Kendall test of monotonic trends (Mann 1945, Kendall 1975), with the Climate Data Toolbox 'mann_kendall' function in MATLAB R2019a (Greene et al. 2019). The application of a non-parametric test was appropriate since the distributions of phenology metrics (e.g. start date and peak date for all years) and month-wise chl *a* (e.g. October chl *a* for all years) were non-normal. For mapped trends, the null hypothesis is that there is no trend in the data over time. No detrending was performed on phenology metric time series, because as single DOY values, these were considered independent data points from year to year. No detrending was performed for month-wise chl *a*, as each month's mean chl *a* was considered an independent data point from year to year.

To determine trends by ecoregion, regionally averaged monthly chl *a* and phenology metrics (1 value per year) were tested for significant trends over time

using a non-parametric Theil-Sen slope test. Detrending was performed to de-seasonalize the overall long-term monthly chl *a* time series (Fig. S12) using the Climate Data Toolbox 'deseason' function in MATLAB R2019a (Greene et al. 2019), which detrends to isolate the seasonal component, then subtracts the seasonal component of the time series from the original data (Fig. S12). No detrending was performed on phenology metric time series, because as single DOY values, these were considered independent data points from year to year. Theil-Sen non-parametric estimates of slope were performed on each ecoregion's de-seasonalized chl *a* to calculate trends. The significance of the trends was assessed with Mann-Kendall tests. The application of a non-parametric test was appropriate since both the de-seasonalized monthly chl *a* (e.g. northern shelf mean chl *a* during every month over the entire time series) and phenology metrics (e.g. northern shelf mean start date and peak date across all years) were not normally distributed. Like the test above, the null hypothesis is that there is no trend in the data over time.

For environmental data, month-wise trends over time and decadal comparisons followed the same statistical methods used for chl *a*. For wind speed, long-term trends in month-wise wind speed were calculated using Theil-Sen non-parametric estimates of slope over time at each *x*,*y* location in m s^{-1} yr^{-1}. Each month's relative trend was calculated as the trend (m s^{-1} yr^{-1}) relative to the long-term mean wind speed (m s^{-1}) at each *x*,*y* location for each month. The significance of month-wise trends was assessed using Mann-Kendall tests. Because trends were calculated for each month of the year, data were purposefully not de-seasonalized prior to trend analysis. For PAR data and SST data, month-wise trends over time were calculated using Theil-Sen non-parametric estimates of slope over time at each *x*,*y* location, and the significance of those trends was assessed using Mann-Kendall tests. To determine the significance of decadal differences in the daily time series of PAR and SST, we applied Kruskal-Wallis tests to compare each DOY mean for 2001–2011 to the same DOY mean for 2012–2022 for each ecoregion. Since we analyzed the seasonal pattern for each decade, we purposefully did not de-seasonalize the data prior to decadal comparisons.

3. RESULTS

3.1. Patterns in seasonal chl *a* timing

Monthly patterns in chl *a* show an overall offshore-to-onshore shift in the location of high chl *a* from September to February (Fig. 2). Offshore, the months of October to December show the highest chl *a*, while over the shelf and coast, January to March experience the highest chl *a*. During the summer and fall (January to April) there is a strong north-to-south gradient of increasing chl *a* with latitude. The highest chl *a* concentrations occur over the southern shelf during the summer months of January and February (Fig. 2).

Phenology metrics, including long-term mean start date and peak date, varied with latitude and distance from shore (Fig. 3, Table 1). The long-term mean timing of the start of the accumulation season showed a smooth spatial pattern from offshore to onshore and from north to south, with start dates for the SPF, MIZ, northern shelf, mid-shelf, and southern shelf occurring in September, October, November, December, and January, respectively (Fig. 3a, Table 1). For peak date, the long-term mean was characterized by similar spatial patterns, although peak dates lagged start dates by approximately 1 to 2 mo. Peak dates ranged from early December in the offshore SPF to mid-February over the southern shelf (Fig. 3b, Table 1).

Decadal seasonal cycles of daily chl *a* shifted later in the season for most ecoregions (Fig. 4, Table 2). In the MIZ, the phytoplankton accumulation season started later and ended earlier in 2012–2022 compared to 2001–2011, shortening the length of the

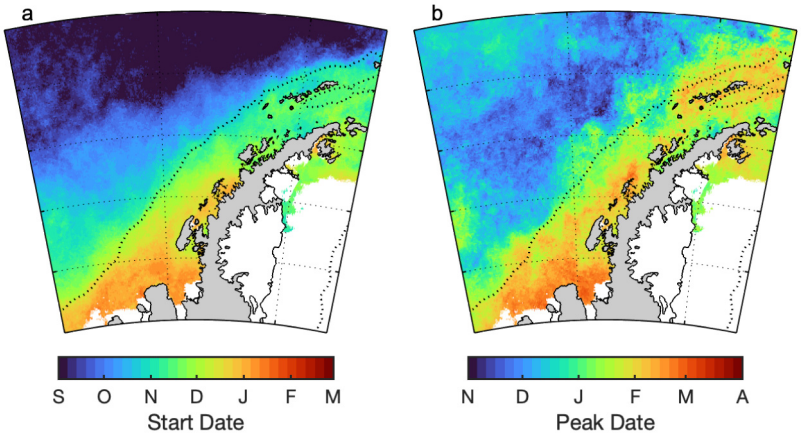

Fig. 3. Long-term mean phenology metrics: (a) start date of the phytoplankton accumulation season via the threshold method, (b) peak date (date of maximum chl *a* concentration). Lettering on color bars indicates the first day of each month (e.g. S = 1 September). Black dotted line indicates the continental shelf break (1000 m isobath)

Table 1. Regional long-term mean phenology metrics. Standard deviations of start date and peak date are in units of days

Ecoregion	Start date	SD	Peak date	SD	Chl *a* (mg m^{-3})			
					Mean	SD	Max.	SD
Southern Polar Front	5 Sep	8	8 Dec	13	0.35	0.04	1.56	0.33
Marginal ice zone	18 Oct	21	17 Dec	21	0.61	0.14	2.87	0.69
Northern shelf	13 Nov	8	22 Jan	13	0.84	0.21	3.57	1.03
Mid-shelf	13 Dec	11	29 Jan	10	1.24	0.34	5.34	1.66
Southern shelf	2 Jan	6	12 Feb	9	1.47	0.54	6.01	2.76

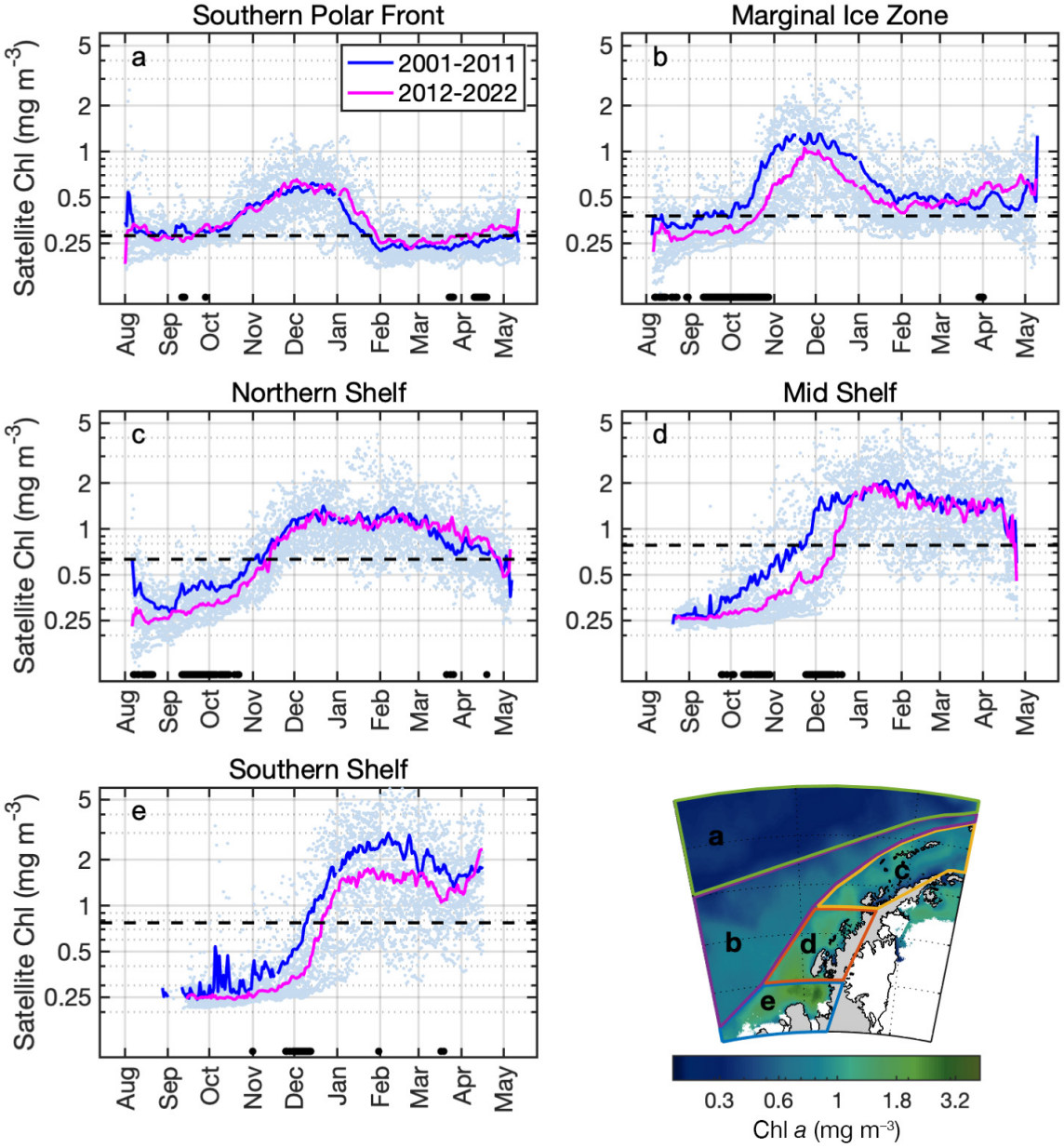

Fig. 4. Seasonal cycles of daily chl *a* concentration for 2 decades: 2001–2011 (blue) vs. 2012–2022 (magenta). Dotted black line indicates the threshold value (long-term median chl *a* + 5%) for each region used to calculate start date. Black circles at lower edges of plots indicate where the difference between decades was statistically significant (Kruskal-Wallis test, $p < 0.05$). Dates refer to the first day of each month (e.g. 'Aug' is 1 August). Regions shown in map inset overlay long-term mean chl *a* concentration

Table 2. Decadal medians and differences between decades for regionally averaged phenology indices. Statistically significant trends (Kruskal-Wallis) are marked with an asterisk (*p < 0.05)

Ecoregion	Start date				Peak date			
	Median 2001–2011	Median 2012–2022	Difference (d)	p	Median 2001–2011	Median 2012–2022	Difference (d)	p
Southern Polar Front	3 Sep	1 Sep	−2	0.880	5 Dec	17 Dec	12	0.257
Marginal ice zone*	9 Oct	26 Oct	17	0.016*	7 Dec	5 Jan	29	0.003*
Northern shelf*	10 Nov	20 Nov	10	0.010*	17 Jan	2 Feb	16	0.034*
Mid-shelf*	7 Dec	26 Dec	19	0.013*	20 Jan	11 Feb	22	0.059
Southern shelf	27 Dec	9 Jan	13	0.151	9 Feb	16 Feb	7	0.364

accumulation season (Fig. 4b). The mid-shelf experienced the largest shift toward later seasonal timing, with the start date becoming later by 19 d from one decade to the next (Fig. 4d). The northern shelf and southern shelf ecoregions showed slightly later timing of chl *a*, with start dates up to 2 wk later in 2012–2022 than in 2001–2011. In the fall season, the strongest shifts toward higher fall chl *a* occurred in the SPF (Fig. 4a) and the northern shelf (Fig. 4c).

Spatially, from 2001–2011 to 2012–2022, the start date of the phytoplankton accumulation season became later along the shelf break and slope (Fig. 5), with decadal differences of to up to 30 d later over parts of the shelf, just offshore of the shelf break, and in most of the MIZ (Fig. 5c). In the far offshore environment, start dates shifted slightly earlier in recent years compared to past years (Fig. 5c). Peak date by decade also shifted later in the season (Fig. 5), with

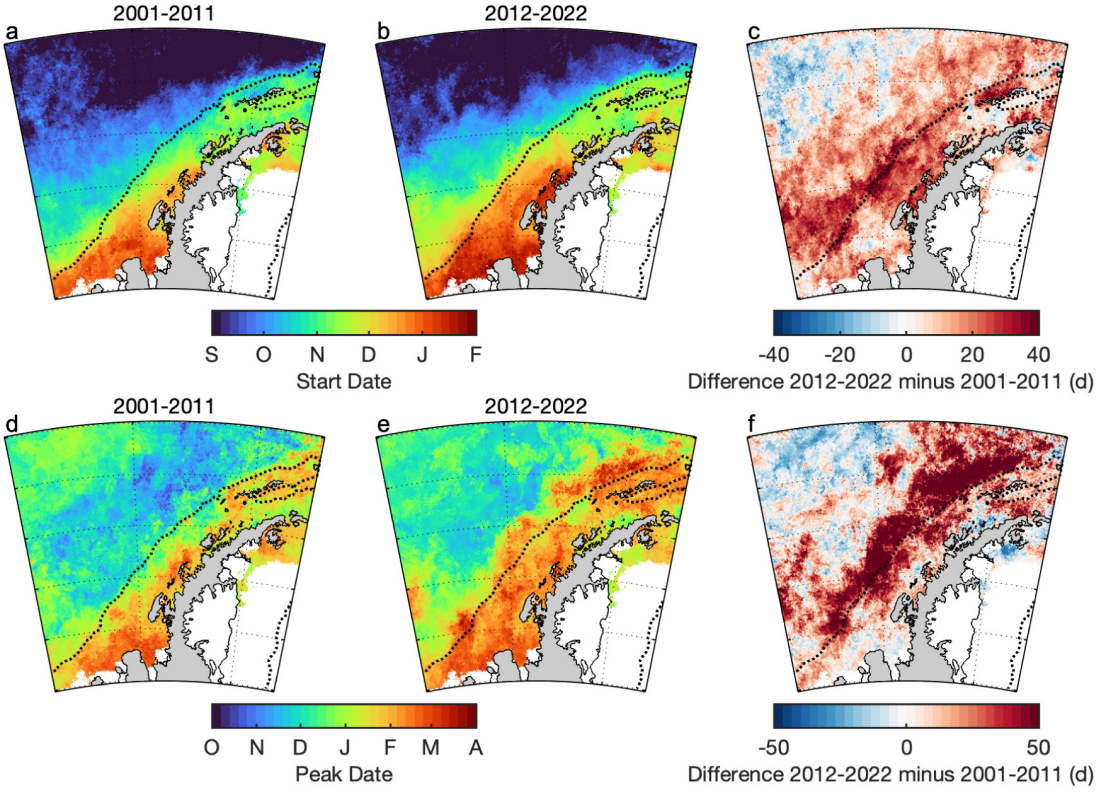

Fig. 5. Decadal mean start dates, peak dates, and decadal differences (days). (a) Mean start date 2001–2011, (b) mean start date 2012–2022, (c) difference (2012–2022 mean start date minus 2001–2011 mean start date), (d) mean peak date 2001–2011, (e) mean peak date 2012–2022, and (f) difference (2012–2022 mean peak date minus 2001–2011 mean peak date) (days). In (c) and (f), blue indicates earlier dates and red indicates later dates in recent years. Black dotted line indicates the continental shelf break (1000 m isobath)

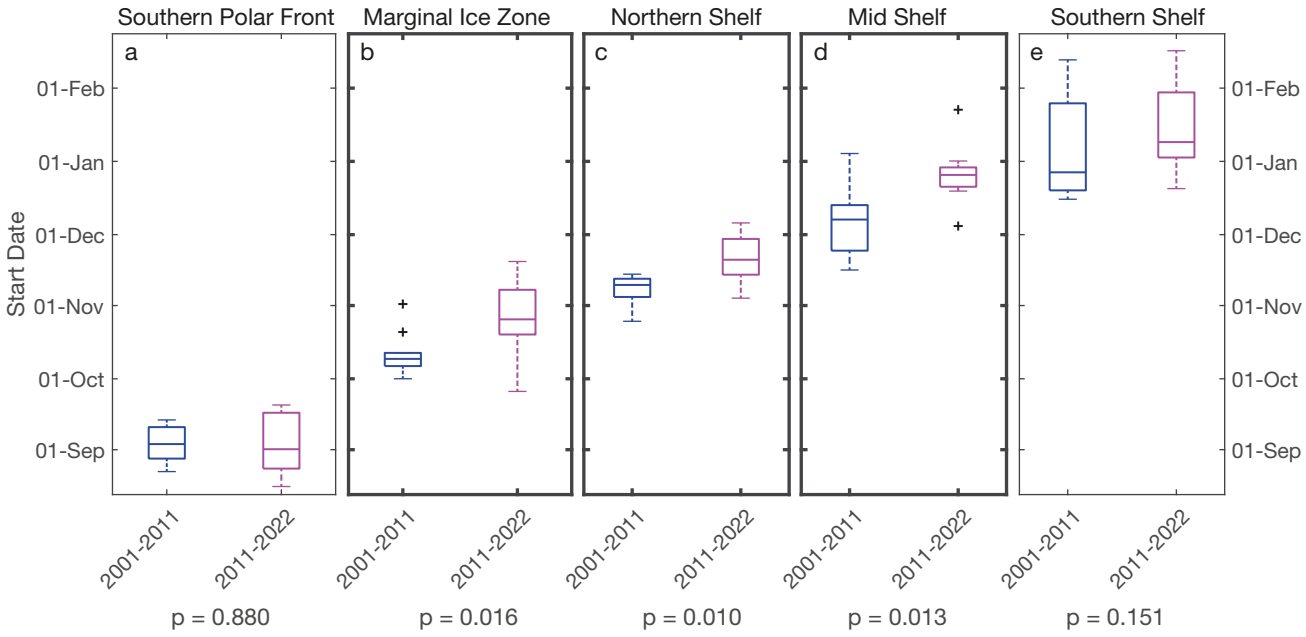

Fig. 6. Median start dates by ecoregion for 2001–2011 (blue) and 2012–2022 (magenta) for (a) Southern Polar Front, (b) marginal ice zone, (c) northern shelf, (d) mid-shelf, and (e) southern shelf. The central line in each box plot is the median, the edges of the box are the 25th and 75th percentiles, whiskers extend to the most extreme data points not considered outliers, and black crosses indicate outliers. Bolded plot outlines indicate ecoregions where decadal differences were statistically significant; p-values were obtained via Kruskal-Wallis tests

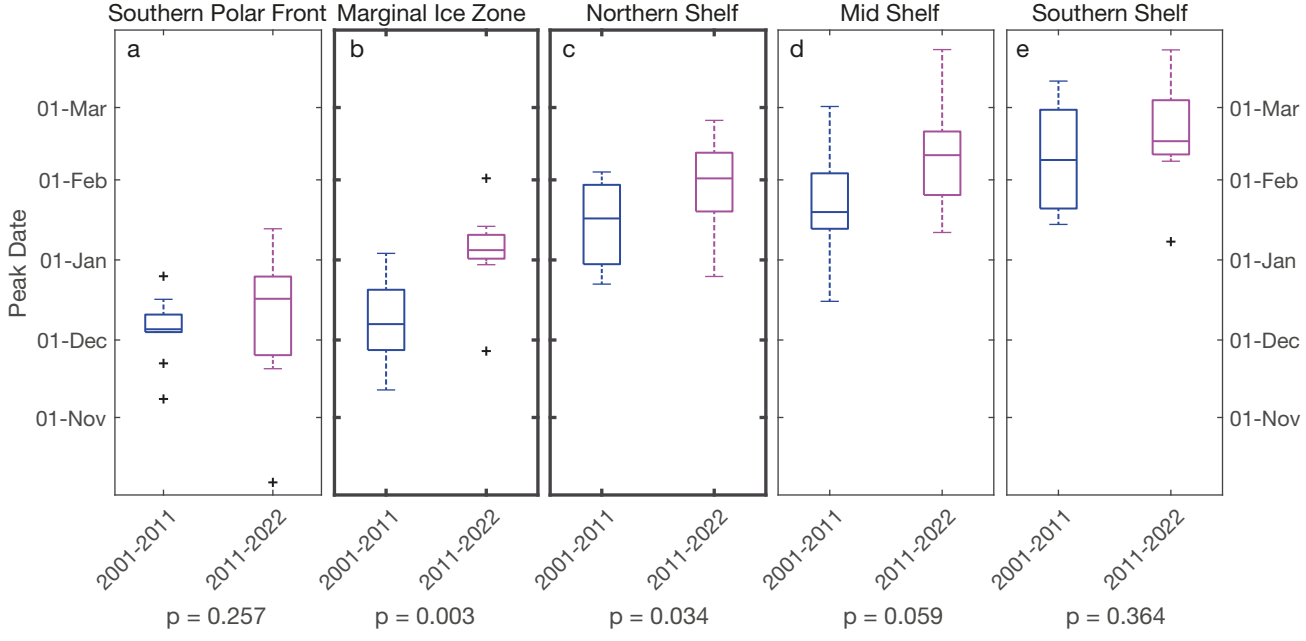

Fig. 7. As in Fig. 6, but for median peak dates

decadal differences of up to 40 d later in 2012–2022 compared to 2001–2011 (Fig. 5c). The shift to later peak dates was spatially most remarkable along and just offshore of the continental shelf break (Fig. 5d–f).

In terms of decadal differences by ecoregion, both start dates and peak dates shifted later in some ecoregions, yet other shifts were not statistically significant (Table 2, Figs. 6 & 7). Start dates were significantly later in recent years compared to past years in the MIZ (Kruskal-Wallis test; chi squared = 5.85, p = 0.016, df = 1), the northern shelf (chi squared = 6.61, p = 0.010, df = 1), and the mid-shelf (chi squared = 6.22,

Table 3. Trends in regionally averaged phenology indices. Statistically significant trends (Mann-Kendall) are marked with an asterisk (*p < 0.05)

Ecoregion	Start date Trend (d yr^{-1})	p	Peak date Trend (d yr^{-1})	p
Southern Polar Front*	−0.435	0.293	1.048	0.007*
Marginal ice zone*	0.595	0.141	1.548	0.018*
Northern shelf	0.381	0.293	0.429	0.293
Mid-shelf	0.848	0.118	1.037	0.183
Southern shelf	0.679	0.154	0.434	0.559

p = 0.013, df = 1) by 10 to 19 d (Table 2, Fig. 6). Peak dates were significantly later in 2012–2022 compared to 2001–2011 in the MIZ (chi squared = 8.69, p = 0.003, df = 1) and the northern shelf (chi squared = 4.48, p = 0.034, df = 1) by 16 and 29 d, respectively (Table 2, Fig. 7). In terms of long-term trends by ecoregion, peak date showed the strongest trends toward later timing in the SPF and MIZ (Table 3), becoming 1 d later per year in the SPF (Theil-Sen slope; Mann-Kendall significance test; p = 0.007) and 1.5 d later per year in the MIZ (p = 0.018).

In terms of mapped long-term trends, the start date of the accumulation season showed diverging trends with low levels of statistical significance (Fig. 8). For the offshore environment (west of 69° W and north of 63° S), there were isolated patches where start dates became earlier over time (Fig. 8a). However, much of the WAP region showed start dates getting later over time (i.e. 49% of the study area; Fig. 8a). Peak dates generally shifted later in the season over time, with an especially strong trend in the MIZ just offshore of the continental shelf break and slope north of 63° S latitude (Fig. 8b).

3.2. Overall satellite-derived chl *a* magnitude trends

Long-term trends from 1997 to 2022 in chl *a* concentration were on the order of ±0.01% yr^{-1} with high annual and interannual variability (Fig. S12), unless resolved on monthly timescales (Fig. 9). By ecoregion, trends over time were minimal with the exception of the SPF (Table 4). Chl *a* increased significantly over time in the SPF (Theil-Sen slope; Mann-Kendall significance test; 0.03% yr^{-1}; p = 0.004) from 1997 to 2022 (Table 4). All other ecoregions showed minimal chl *a* trends over time (up to ±0.02% yr^{-1} at most) with no statistical significance (p > 0.198) (Table 4).

On monthly timescales, long-term chl *a* trends over time were larger in magnitude, decreasing over time in spring (October to November) and increasing over time in summer and fall (January to April) (Fig. 9). October and November showed evidence of strongly decreasing chl *a* in the offshore to outer continental shelf regions, reaching −4 and −5% yr^{-1}, respectively (Fig. 9b,c). January, February, March, and April all showed slight increasing trends in chl *a* on the order of 1 to 4% yr^{-1} (Fig. 9e–h). In summer and fall, statistically significant increases were located mostly offshore of the continental shelf. Nearshore waters showed more variability in the direction of the trends from January through April.

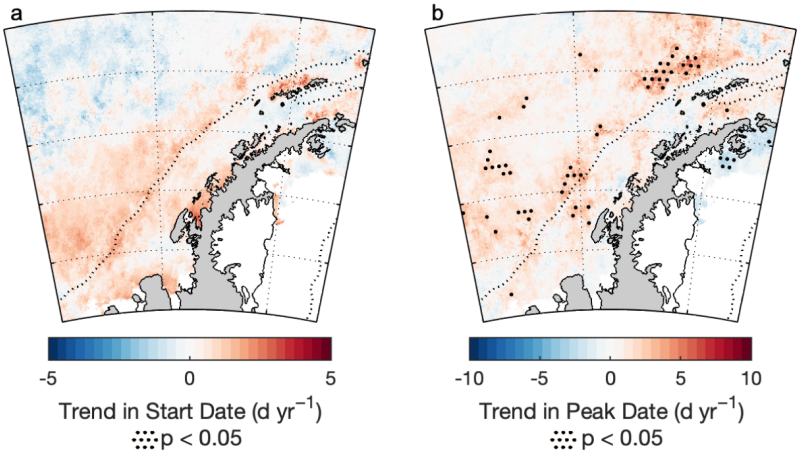

Fig. 8. Trends in (a) start date and (b) peak date of the phytoplankton accumulation season over time, in units of days per year (Theil-Sen slope). Red (blue) indicates a later (earlier) date over time. Black stippling indicates areas where trends are statistically significant (p < 0.05; Mann-Kendall). Black dotted line indicates the continental shelf break (1000 m isobath)

3.3. Trends in environmental variables

Wind speed trends for 1997 to 2022 in individual months showed different long-term trends in separate parts of the seasonal cycle. Wind speed increased over time most notably for the month of November (Fig. 10). Spring months (September, October, and November) showed increasing wind speed over time, whereas the summer months December and January showed slight decreasing trends in wind speed. Fall months displayed mixed trends, with February and March experiencing increasing wind speed over time while April showed decreasing wind speed

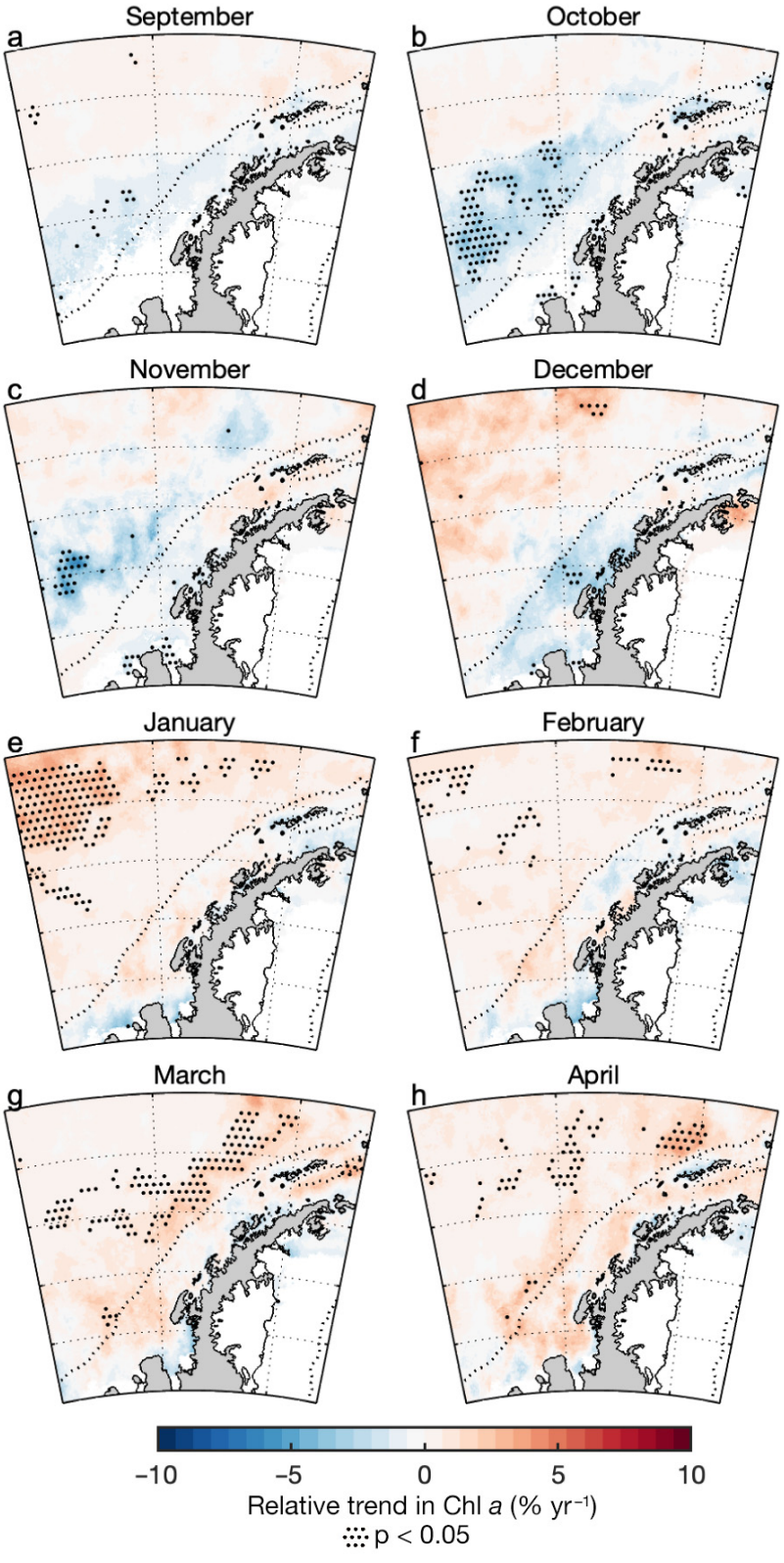

Fig. 9. Trends in chl *a* by month relative to the long-term mean chl *a* for each spatial point for each month over the 25 yr time series (Theil-Sen slope). Black stippling indicates areas where trends are statistically significant ($p < 0.05$; Mann-Kendall). Black dotted line indicates the continental shelf break (1000 m isobath)

over time (Fig. 10). While there was an overall increase in wind speed from 2001–2011 to 2012–2022, especially in the offshore environment, wind direction did not show a substantial change and remained predominantly northwesterly throughout the time series (Fig. S13).

Analysis of PAR and SST data for 1997–2022 did not reveal meaningful trends. We found that the seasonal patterns in PAR were not significantly different between decades for any ecoregion (Fig. S14). By month, trends in PAR showed slight decreases over time (Fig. S15), yet the seasonality of the PAR decreases did not correspond with the seasonality of the chl *a* trends observed (Fig. 9). Likewise, no significant difference was seen in the seasonal cycle of SST between decades (Fig. S16). By month, SST trends showed Septembers becoming slightly warmer, with no other significant trends in any other month in any ecoregion (Fig. S17).

4. DISCUSSION

4.1. Assessing seasonality of phytoplankton

Although the 'spring bloom' has been characterized for nearly 100 yr (Gran & Braarud 1935), studies of phytoplankton phenology in the global ocean differ on the most representative definition of the start date according to different metrics of bloom initiation. Most biomass-based estimates customarily point to the spring season as the start of the phytoplankton accumulation season rather than winter, varying depending on nutrient availability, latitude, and climatological factors. Often, start date co-occurs with the physical stratification of the water column (Sverdrup 1953, Siegel et al. 2002). Some argue that the seasonal cycle of phytoplankton growth truly begins in winter when conditions are well-mixed, according to the dilu-

Table 4. Trends in regionally averaged, de-seasonalized monthly chlorophyll *a* (chl *a*). Statistically significant trends (Mann-Kendall) are marked with an asterisk (*p < 0.05)

Ecoregion	Monthly chl *a*		
	Trend (mg m^{-3} yr^{-1})	Relative trend (% yr^{-1})	p
Southern Polar Front*	0.00007	0.02	0.0004*
Marginal ice zone	−0.00002	−0.003	0.743
Northern shelf	−0.00007	−0.01	0.198
Mid-shelf	−0.00009	−0.009	0.355
Southern shelf	−0.0001	−0.009	0.227

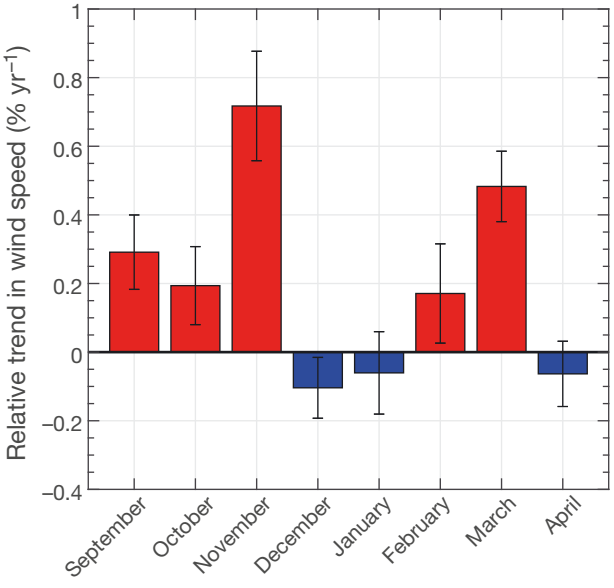

Fig. 10. Relative trends in wind speed by month averaged for the Southern Polar Front (SPF) ecoregion 1997–2022 from ERA5 (Theil-Sen slope). Relative trends were normalized to the long-term mean wind speed at each *x,y* location for each month. Error bars indicate spatial standard deviation of trends over time

tion hypothesis (Behrenfeld & Boss 2014). Due to limited information about loss rates (i.e. grazing, viruses, sinking) over the time and space scales needed for this analysis, in this paper we focus on phytoplankton accumulation, the seasonal period of increasing phytoplankton biomass (as measured by surface chl *a* concentration) when the average phytoplankton mass-specific loss rates are smaller than growth rates (Evans & Parslow 1985, Banse 1992, Behrenfeld & Boss 2018, Arteaga et al. 2020). Many studies also calculate the timing of the phytoplankton accumulation season start date based on biomass increase, such as the date when chl *a* rises above a pre-defined threshold value (Siegel et al. 2002, Racault et al. 2012). Other approaches use the timing of the peak in the daily rate of change, the date when the cumulative sum of chl *a* rises above a certain value, and the date of the largest step change in the cumulative sum of anomalies in chl *a* (Brody et al. 2013, Thomalla et al. 2015). Through a sensitivity analysis evaluating a variety of published metrics, we demonstrate that our methods and conclusions applying the threshold metric are robust (Fig. S10).

4.2. Decadal shifts in bloom phenology

Phytoplankton accumulation season start dates and peak dates are shifting later in the season, and chl *a* is remaining higher for longer into the fall season (Figs. 4, 5, & 9). Start date is occurring later over time especially in the MIZ and over the shelf (Figs. 4b, 5c, & 6), and peak date is becoming later over time especially just offshore of the shelf break (Figs. 5f, 7, & 8). Decadal differences may be muted slightly (Figs. 6 & 7) when averaged over space and time, as the averaging likely masks the strong trends seen along the continental shelf break in the MIZ (Fig. 5). Chl *a* trends by month further support the shift toward later timing each season, as October and November show long-term decreases in chl *a*, while January to April show long-term increases in chl *a* (Fig. 9). Although global climate models predict earlier spring blooms in polar regions, we saw a shift toward later spring start dates and later summer peak dates over time in the WAP region.

While the timing of the phytoplankton accumulation season is generally shifting later, by ecoregion, phenology is trending in mixed directions. Our results reveal that offshore open-ocean spring blooms are shifting earlier while blooms in ice-associated ecoregions shift later. These results are not mutually exclusive, and both can occur simultaneously. The open ocean environment of the SPF is very different from the MIZ and shelf, since the latter environments experience sea ice coverage for a substantial portion of the year. The different level of exposure to sea ice may contribute to the different trends in phytoplankton phenology for the open-ocean environment compared to the ice-influenced ecoregions. These diverging trends represent a temporal widening in the bloom timing between the open-ocean environment and the ice-influenced environment. If this divergence continues in future years, ecological consequences could further differentiate these 2 systems as the effects of the shifting bloom timing propagate throughout the marine food web.

4.3. Potential mechanisms for seasonal shifts

Possible drivers behind observed seasonal shifts in timing include changes in wind speed, cloud cover, temperature, and sea ice dynamics. Wind speed is the most likely mechanism for the observed change in spring start dates (Fig. 10). A long-term increase in wind mixing has likely decreased early-season water column stability, suppressing phytoplankton accumulation (Fig. 11). Other available environmental data (i.e. PAR, SST) cannot explain the patterns observed in shifting chl *a* phenology.

4.3.1. Increased spring wind speed

Wind speed trends for 1997–2022 in individual months support the idea that enhanced winds could suppress an early spring bloom in the WAP. Wind speed is increasing over time for the month of November (Fig. 10), concurrent with October and November showing later phytoplankton accumulation season start dates (Fig. 9). Our observations of increasing wind speed are consistent with other findings that spring (September–November) wind speed is increasing over time for the broader West Antarctica sector of the Southern Ocean (Yu et al. 2020). Due to increased spring wind speeds in recent years, seasonal water column stratification from sea ice melt may not be occurring early enough to support an early spring bloom. Although there is evidence of a shallowing summer MLD over time based on the month of January (Brown et al. 2019), it is nevertheless possible that the onset of the spring MLD shallowing is now happening later in the season each year. For the WAP, as the system progresses toward lower sea ice extent and shorter sea ice duration, wind mixing may be possible throughout more of each year in a low-ice state. A similar relationship between ice retreat, high wind speeds, and later bloom initiation was seen in the Bering Sea, a polar system experiencing long-term declines in seasonal sea ice. In years with early sea ice retreat (boreal early spring, before mid-March), the spring phytoplankton bloom was delayed until the water columns stratified with warming air temperatures and increased sunlight (Stabeno et al. 2001, 2012).

We developed a conceptual diagram for the difference between past conditions and recent conditions in the MIZ in spring to contextualize our results (Fig. 11). In spring, in the MIZ, the past had lower wind speeds, resulting in a shallower MLD. Light-limitation depth in this conceptual diagram is illustrated as a range of depths falling between the shallower critical depth definition of Sverdrup (1953) with a liberal compensation irradiance, and a more conservative deeper light-

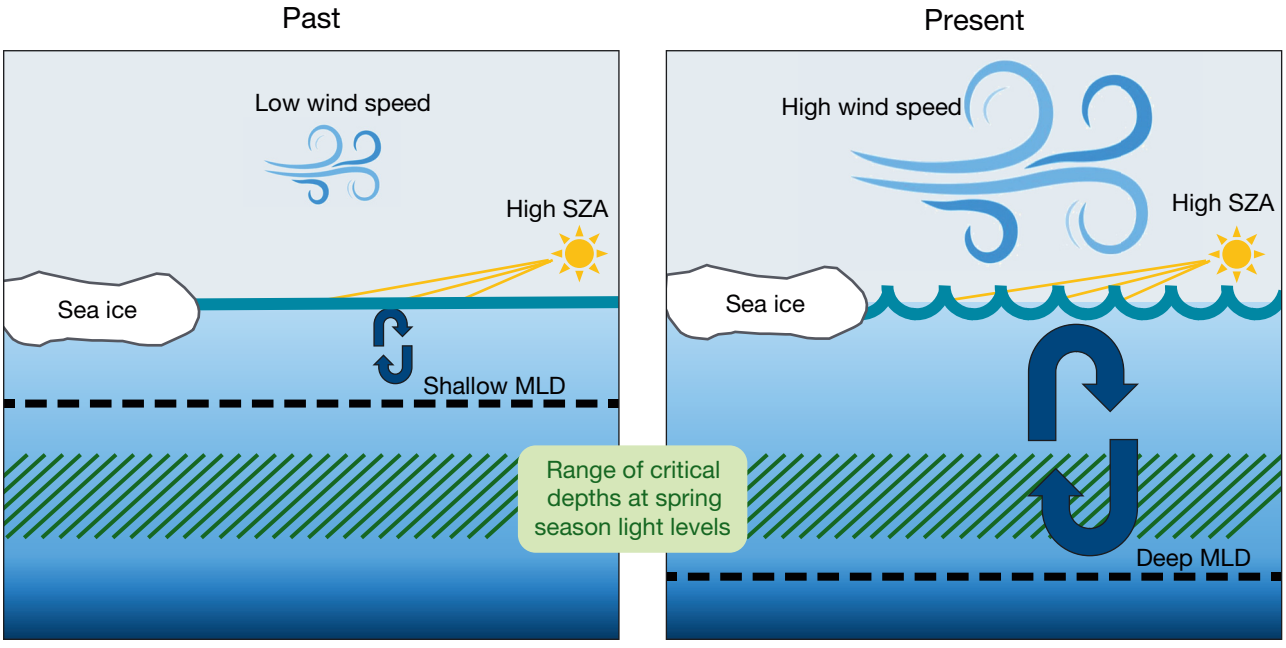

Fig. 11. Conceptual diagram illustrating past conditions vs. present conditions in the marginal ice zone west of the Antarctic Peninsula in the spring season (October to November). Spring conditions are inherently light-limited due to low solar zenith angles (SZA). Past conditions with lower wind speeds and shallower mixed layer depth (MLD) provided more favorable conditions for spring surface phytoplankton accumulation compared to present conditions

limitation depth corresponding to a smaller compensation irradiance (Geider et al. 1986, Behrenfeld & Boss 2018). With increased wind speeds under present conditions, MLD deepens. Increased spring wind speeds over time are especially prevalent in the month of November (Fig. 10). However, we found no long-term change in PAR (Figs. S14 & S15). Spring conditions are inherently light limited due to high solar zenith angles at these high latitudes. At the same spring light levels, with the MLD deepening due to higher wind speeds and less water column stability, phytoplankton are likely more light-limited under present conditions compared to the past.

4.3.2. Other environmental data fail to explain seasonal chl *a* shifts

Other potential mechanisms for later start dates include (1) a reduction in PAR due to increased cloud cover or (2) a shift in SST. Previous studies have shown evidence of a long-term increase in cloud cover and precipitation over the WAP (Kirchgäßner 2010, 2011, Datta et al. 2019, Sato & Simmonds 2021). Cloudier conditions with lower PAR would further limit an earlier start to the phytoplankton accumulation season if combined with enhanced wind mixing. Temperature acts as a major control on phytoplankton phenology in the global ocean, including the growth preference for different species and the length of the phytoplankton accumulation season in different ocean biomes (Racault et al. 2012, Poloczanska et al. 2016, van Leeuwe et al. 2020). Shifts in SST could therefore theoretically alter the start date and peak date of the accumulation season. However, according to our analysis, long-term change in the seasonal timing of PAR (Figs. S14 & S15) and SST (Figs. S16 & S17) are not driving factors for the observed shifts in chl *a* phenology.

One final potential mechanism for later phytoplankton timing may be sea ice decline. A decrease in sea-ice-melt-induced water column stability would suppress spring phytoplankton accumulation. However, this sea ice explanation may be confounded by other factors. Venables et al. (2013) presented evidence that the timing of bloom initiation in the WAP follows light availability rather than sea ice retreat, and that low- and high-ice years showed similar bloom initiation dates. Our results support this idea, as the progression toward later start dates is not clearly mirrored by a progression toward later sea ice retreat over the same set of corresponding years (Fig. S18). It is possible that the lack of correlation between spring chl *a* trends and sea ice trends is due to the potential that satellites now miss the earliest ice-edge bloom. In slope and offshore waters, the ice-edge bloom occurred later in the season in past decades. In recent years, if the ice-edge bloom is occurring in late winter or early spring before satellites have sufficient sun angle to collect reliable data, e.g. August (Fig. 2), satellites cannot capture the earliest bloom. In that case, our results indicate that the non-ice-edge bloom is beginning later over time (Fig. 4), implying that the later phytoplankton accumulation timing is not directly associated with changes in sea ice dynamics. Fluctuations in sea ice dynamics are linked to oscillations of the Southern Annular Mode (SAM) and changes in wind speed and direction (Stammerjohn et al. 2003, 2008, Turner et al. 2013). Our results show increasing wind speed over the offshore waters from the northwest, consistent with a long-term trend toward a positive SAM, without a concurrent change in wind direction (Fig. S13). As the region experiences future shifts in sea ice extent and duration, future interactions between the SAM, wind speed, sea ice, and phytoplankton merit further study.

4.4. Ecological impacts of shifting phenology

Phytoplankton represent the base of this dynamic food web; thus, shifts in phytoplankton seasonal timing may impact the feeding, migration, and breeding behaviors of higher trophic level organisms. The MIZ provides critical habitat for krill, fishes, seabirds, pinnipeds, and cetaceans. While krill may have the ability to shift their phenology in response to interannual variability in environmental conditions (Conroy et al. 2023), the relative abundance of other taxa such as salps and pteropods can enhance grazing pressure on phytoplankton (Bernard et al. 2012). Zooplankton grazing can act as an important control on phytoplankton bloom duration as seen in other parts of coastal Antarctica (Kauko et al. 2021), and thus effects of changes in grazing on phytoplankton phenology in the WAP region merit further study. Changing phenology at the base of the food web could additionally disrupt the life history strategies of keystone species such as Antarctic silverfish, Adélie penguins, and humpback whales (Fraser et al. 1992, Saba et al. 2014, Weinstein & Friedlaender 2017, Cimino et al. 2019, 2023, Henley et al. 2019, Corso et al. 2022).

The results of the present study suggest that start dates and peak dates of the phytoplankton accumulation season are occurring later in the MIZ and that fall phytoplankton biomass is persisting later in the season over time over the northern continental shelf. Spring shifts and fall shifts may have different eco-

logical implications. In spring, overall the WAP ecosystem is less 'predictable' during years with earlier spring sea ice retreat when the timing of phenological events throughout the food web is more diverse (i.e. higher variability in timing) (Cimino et al. 2023). This implies that as the system experiences further sea ice decline in future years, the timing of events in spring may become increasingly variable. In fall, higher chl *a* concentrations in recent years (Figs. 4 & 9) could provide a sustained food source for zooplankton and higher trophic levels later into the season than in past years. This shift toward a highly productive fall season in recent years could have implications for higher trophic level organism life history strategies.

4.5. Impact on annual carbon uptake

Results imply that annual biological carbon uptake may not be changing substantially over time based on 1997–2022, because both spring and fall processes are shifting later in the season and the overall trend in chl *a* is minimal. While the timing of events each season is shifting later in the season over time, the total magnitude of chl *a* is only minimally changing over time (Fig. S9). In the middle of the austral summer, the generally increasing chl *a* trend observed in January in the present study (Fig. 9e) corresponds with the results of Brown et al. (2019) showing increasing *in situ* chl *a* based on data collected during summer months. Furthermore, the statistically significant chl *a* increases in the SPF (Table 4) align with the overall 'greening' of the Southern Ocean observed by Del Castillo et al. (2019) and Pinkerton et al. (2021). This offshore environment is quite different from the coastal WAP ecoregions in that it is typically defined as a high nutrient–low chlorophyll ecosystem and is considered to be an oligotrophic area (Tréguer & Jacques 1992), with long-term mean chl *a* concentrations ≤0.4 mg m^{-3} (Fig. S12). The results of the present study show smaller-magnitude chl *a* trends than those presented by Montes-Hugo et al. (2009), which likely had significant biases using the older CZCS data (Figs. S1 & S2). Generally, small-magnitude changes in chl *a* suggest that despite the warming temperatures and generally lower sea ice conditions compared to the past, the WAP is not experiencing long-term declines in phytoplankton biomass.

Changes in the timing of the phytoplankton accumulation season may affect the timing and magnitude of biological CO_2 uptake. Biological production drives variability in air–sea CO_2 exchange along the WAP (Carrillo et al. 2004, Eveleth et al. 2017). Since the mid-2000s, several studies utilizing pCO_2 observations have suggested a strengthening of Southern Ocean CO_2 uptake (Xue et al. 2015, Landschützer et al. 2015, Munro et al. 2015b). However, the seasonal timing of when this strengthening is occurring is still unknown. Our results suggest that austral fall may be experiencing higher chl *a* concentration than in the past (Figs. 4 & 9), possibly strengthening CO_2 uptake in the fall months. Overall, the amplitude of the seasonal cycle in surface pCO_2 is small, because the thermal and biological components of the seasonal cycle balance one another (Munro et al. 2015a). This suggests that at the seasonal scale, impacts of warm summer temperatures on carbon uptake are balanced by biological CO_2 uptake. Phytoplankton phenology shifts show later spring start dates and higher fall chl *a*, but this shift is seen in the timing of the biological carbon uptake rather than the magnitude. The connection between chl *a* and carbon cycling depends on many factors other than the magnitude of the bloom or its timing (Henley et al. 2020). For example, chl *a* often increases before phytoplankton carbon in the Southern Ocean spring bloom (Vives et al. 2023). Whether there has been a change in the total annual carbon uptake based on changing chl *a* timing remains to be seen and merits further study. Our results imply that phytoplankton biomass is not changing in the long term despite phenological shifts toward later start date in spring and higher chl *a* in fall.

4.6. Future outlook

Changing chl *a* phenology may relate to changing phytoplankton community composition. Although data from Palmer Station (in the mid-shelf ecoregion in this study) show diatoms as the first species to bloom (Nardelli et al. 2023), other studies find that the haptophyte *Phaeocystis antarctica* is the dominant first bloomer, not diatoms, especially in offshore waters from the continental shelf break outwards (Arrigo et al. 2017, Joy-Warren et al. 2019). Because the strongest shifts in the timing of start date and peak date are occurring along the continental shelf break in our results (Fig. 5), it is possible that these changes are affecting haptophytes, but more work is needed to discern phytoplankton species with temporal coverage over the entire season. Future work will explore algorithms to leverage upcoming hyperspectral satellite missions (Dierssen et al. 2021) to remotely detect different phytoplankton groups going forward in this dynamic and rapidly changing region of the Southern Ocean.

Continued long-term *in situ* monitoring is critical to maintain in this region to further validate remote sensing algorithms and explore potential new technologies for assessing biodiversity and biogeochemistry. High solar zenith angle at high latitudes in the southern hemisphere limit temporal coverage of passive ocean color measurements, making winter months May to August unretrievable (Fig. 2; Fig. S7) and early spring and late fall retrievals (September, April) more prone to error due to the longer pathlength through Earth's atmosphere. Additionally, satellite-derived chl *a* estimates only apply during cloud-free conditions and only in the surface ocean. Studies show that chl *a* maximum concentrations often occur at depths as deep as 75 to 100 m that cannot be assessed directly with passive ocean color measurements (Holm-Hansen & Hewes 2004). These biases can be mitigated in future work using data from profiling biogeochemical-Argo floats (e.g. Arteaga et al. 2020, Hague & Vichi 2021) and airborne and space-based lidar to better understand what happens in Antarctic waters at times and depths for which passive satellite observations are not available. Space-based lidar has the potential to estimate phytoplankton biomass within the first 3 optical depths for more representative phytoplankton physiology measurements from space (Behrenfeld et al. 2017). Thus, merging field data and advanced modeling (Kim et al. 2021) with new technology, such as hyperspectral drones (Joyce et al. 2019) and airborne and space-based lidar (Behrenfeld et al. 2017, Bisson et al. 2021), will allow us to better explore changes in this dynamic region. Future work will also be improved by the increasing length of the time series. Although 25 yr of ocean color data represent a valuable resource, the time series is still relatively short. Modeling studies have revealed that at high latitudes, 20 to 40 yr of data are needed to illuminate climate-relevant trends in ocean primary production (Henson et al. 2013, 2018). With the launch of the next generation of hyperspectral satellite missions like NASA's Plankton, Aerosols, Clouds, and ocean Ecosystems and Surface Biology and Geology over the next decade (Dierssen et al. 2023), we will continue to investigate these long-term bloom phenology trends and impacts on the trophic web in this dynamic polar ecosystem.

Data availability. Ocean color data used in satellite-derived chl *a* analysis are available from CMEMS at https://data.marine.copernicus.eu/product/OCEANCOLOUR_GLO_BGC_L4_MY_009_104/services (data set: Cmems_obs-oc_glo_bgc-plankton_my_l4-gapfree-multi-4km_p1d). Wind data are available from ECMWF via the Copernicus Climate Data Store at https://cds.climate.copernicus.eu/cdsapp#!/dataset/reanalysis-era5-single-levels?tab=form (data set: ERA5 hourly data on single levels from 1940 to present). PAR data are available from NASA ocean color web at https://oceancolor.gsfc.nasa.gov/ (data set: Photosynthetically Available Radiation [PAR]). SST data are available from CMEMS at https://data.marine.copernicus.eu/product/SST_GLO_SST_L4_REP_OBSERVATIONS_010_011/services (data set: METOFFICE-GLO-SST-L4-REP-OBS-SST). Code used to make figures is available at https://doi.org/10.5281/zenodo.10790613 (Turner 2024).

Acknowledgements. Funding for this work was provided by NASA Interdisciplinary Science (IDS) award number 80NSSC20K1518 and NSF Office of Polar Programs Postdoctoral Fellowship to J.S.T. (award number 2317774). Additional funding came from Palmer Long Term Ecological Research grant NSF LTER-2026045. Mapping help was provided by Schuyler Nardelli and Jack Conroy. We thank E. Boss, M. Pinkerton, and 3 anonymous reviewers for their helpful comments during the peer-review process.

LITERATURE CITED

Arrigo KR, McClain CR (1994) Spring phytoplankton production in the western Ross Sea. Science 266:261–263

Arrigo KR, van Dijken G, Long M (2008) Coastal Southern Ocean: a strong anthropogenic CO_2 sink. Geophys Res Lett 35:L21602

Arrigo KR, van Dijken GL, Alderkamp AC, Erickson ZK and others (2017) Early spring phytoplankton dynamics in the western Antarctic Peninsula. J Geophys Res Oceans 122:9350–9369

Arteaga LA, Boss E, Behrenfeld MJ, Westberry TK, Sarmiento JL (2020) Seasonal modulation of phytoplankton biomass in the Southern Ocean. Nat Commun 11:5364

Babin M, Morel A, Gentili B (1996) Remote sensing of sea surface sun-induced chlorophyll fluorescence: consequences of natural variations in the optical characteristics of phytoplankton and the quantum yield of chlorophyll *a* fluorescence. Int J Remote Sens 17:2417–2448

Banse K (1992) Grazing, temporal changes of phytoplankton concentrations, and the microbial loop in the open sea. In: Falkowski PG, Woodhead AD, Vivirito K (eds) Primary productivity and biogeochemical cycles in the sea. Environmental Science Research, Vol 43. Springer, Boston, MA, p 409–440

Barbieux M, Uitz J, Bricaud A, Organelli E and others (2018) Assessing the variability in the relationship between the particulate backscattering coefficient and the chlorophyll *a* concentration from a global Biogeochemical-Argo database. J Geophys Res Oceans 123:1229–1250

Behrenfeld MJ, Boss ES (2014) Resurrecting the ecological underpinnings of ocean plankton blooms. Annu Rev Mar Sci 6:167–194

Behrenfeld MJ, Boss ES (2018) Student's tutorial on bloom hypotheses in the context of phytoplankton annual cycles. Glob Change Biol 24:55–77

Behrenfeld MJ, Hu Y, O'Malley RT, Boss ES and others (2017) Annual boom–bust cycles of polar phytoplankton biomass revealed by space-based lidar. Nat Geosci 10:118–122

Bernard KS, Steinberg DK, Schofield OME (2012) Summertime grazing impact of the dominant macrozooplankton

off the Western Antarctic Peninsula. Deep Sea Res I 62: 111–122
Bisson KM, Boss E, Werdell PJ, Ibrahim A, Behrenfeld MJ (2021) Particulate backscattering in the global ocean: a comparison of independent assessments. Geophys Res Lett 48:e2020GL090909
Boss E, Behrenfeld M (2010) In situ evaluation of the initiation of the North Atlantic phytoplankton bloom. Geophys Res Lett 37:L18603
Brody SR, Lozier MS, Dunne JP (2013) A comparison of methods to determine phytoplankton bloom initiation. J Geophys Res Oceans 118:2345–2357
Brown MS, Munro DR, Feehan CJ, Sweeney C, Ducklow HW, Schofield OM (2019) Enhanced oceanic CO_2 uptake along the rapidly changing West Antarctic Peninsula. Nat Clim Change 9:678–683
Carrillo CJ, Smith RC, Karl DM (2004) Processes regulating oxygen and carbon dioxide in surface waters west of the Antarctic Peninsula. Mar Chem 84:161–179
Carvalho F, Kohut J, Oliver MJ, Sherrell RM, Schofield O (2016) Mixing and phytoplankton dynamics in a submarine canyon in the West Antarctic Peninsula. J Geophys Res Oceans 121:5069–5083
Chapman CC, Lea MA, Meyer A, Sallée JB, Hindell M (2020) Defining Southern Ocean fronts and their influence on biological and physical processes in a changing climate. Nat Clim Change 10:209–219
Cimino MA, Patterson-Fraser DL, Stammerjohn S, Fraser WR (2019) The interaction between island geomorphology and environmental parameters drives Adélie penguin breeding phenology on neighboring islands near Palmer Station, Antarctica. Ecol Evol 9:9334–9349
Cimino MA, Conroy JA, Connors E, Bowman J and others (2023) Long-term patterns in ecosystem phenology near Palmer Station, Antarctica, from the perspective of the Adélie penguin. Ecosphere 14:e4417
Cleveland JS, Perry MJ, Kiefer DA, Talbot MC (1989) Maximal quantum yield of photosynthesis in the northwestern Sargasso Sea. J Mar Res 47:869–886
Conroy JA, Steinberg DK, Thomas MI, West LT (2023) Seasonal and interannual changes in a coastal Antarctic zooplankton community. Mar Ecol Prog Ser 706:17–32
Copernicus Climate Change Service (2018) ERA5: Fifth generation of ECMWF atmospheric reanalyses of the global climate. https://cds.climate.copernicus.eu/cdsapp#!/home (accessed 25 April 2022)
Corso AD, Steinberg DK, Stammerjohn SE, Hilton EJ (2022) Climate drives long-term change in Antarctic Silverfish along the western Antarctic Peninsula. Commun Biol 5: 104
Danziger Z (2024) Theil-Sen robust linear regression. MATLAB Central File Exchange. https://www.mathworks.com/matlabcentral/fileexchange/48294-theil-sen-robust-linear-regression
Datta RT, Tedesco M, Fettweis X, Agosta C, Lhermitte S, Lenaerts JTM, Wever N (2019) The effect of foehn-induced surface melt on firn evolution over the Northeast Antarctic Peninsula. Geophys Res Lett 46:3822–3831
Del Castillo CE, Signorini SR, Karaköylü EM, Rivero-Calle S (2019) Is the Southern Ocean getting greener? Geophys Res Lett 46:6034–6040
Dierssen HM (2000) Ocean color remote sensing of chlorophyll and primary production west of the Antarctic Peninsula. PhD dissertation, University of California, Santa Barbara, CA
Dierssen HM, Smith RC (2000) Bio-optical properties and remote sensing ocean color algorithms for Antarctic Peninsula waters. J Geophys Res 105:26301–26312
Dierssen HM, Vernet M, Smith RC (2000) Optimizing models for remotely estimating primary production in Antarctic coastal waters. Antarct Sci 12:20–32
Dierssen HM, Smith RC, Vernet M (2002) Glacial meltwater dynamics in coastal waters west of the Antarctic peninsula. Proc Natl Acad Sci USA 99:1790–1795
Dierssen HM, Ackleson SG, Joyce KE, Hestir EL, Castagna A, Lavender S, McManus MA (2021) Living up to the hype of hyperspectral aquatic remote sensing: science, resources and outlook. Front Environ Sci 9:649528
Dierssen HM, Gierach M, Guild LS, Mannino A and others (2023) Synergies between NASA's hyperspectral aquatic missions PACE, GLIMR, and SBG: opportunities for new science and applications. J Geophys Res Biogeosci 128: e2023JG007574
Evans GT, Parslow JS (1985) A model of annual plankton cycles. Biol Oceanogr 3:327–347
Eveleth R, Cassar N, Doney SC, Munro DR, Sweeney C (2017) Biological and physical controls on O_2/Ar, Ar and pCO_2 variability at the Western Antarctic Peninsula and in the Drake Passage. Deep Sea Res II 139:77–88
Fenchel T (1988) Marine plankton food chains. Annu Rev Ecol Syst 19:19–38
Fraser WR, Trivelpiece WZ, Ainley DG, Trivelpiece SG (1992) Increases in Antarctic penguin populations: reduced competition with whales or a loss of sea ice due to environmental warming? Polar Biol 11:525–531
Friedland KD, Mouw CB, Asch RG, Ferreira ASA and others (2018) Phenology and time series trends of the dominant seasonal phytoplankton bloom across global scales. Glob Ecol Biogeogr 27:551–569
Frouin R, Pinker RT (1995) Estimating photosynthetically active radiation (PAR) at the Earth's surface from satellite observations. Remote Sens Environ 51:98–107
Frouin R, Franz BA, Werdell PJ (2002) The SeaWiFS PAR product. In: Hooker SB, Firestone ER (eds) Algorithm updates for the Fourth SeaWiFS data reprocessing. NASA Tech Memo 2003-206892, Vol 22. NASA Goddard Space Flight Center, Greenbelt, MD, p 46–50
Frouin R, McPherson J, Ueyoshi K, Franz BA (2012) A time series of photosynthetically available radiation at the ocean surface from SeaWiFS and MODIS data. In: Frouin R, Ebuchi N, Pan D, Saino T (eds) Proc SPIE 8252. Remote sensing of the marine environment II. SPIE Asia-Pacific Remote Sensing, 29 October–1 November 2012, Kyoto, Japan, art. no. 852519
Garnesson P, Mangin A, D'Andon OF, Demaria J, Bretagnon M (2019) The CMEMS GlobColour chlorophyll *a* product based on satellite observation: multi-sensor merging and flagging strategies. Ocean Sci 15:819–830
Geider RJ, Osbonie BA, Raven JA (1986) Growth, photosynthesis, and maintenance metabolic cost in the diatom *Phaeodactylum tricornutum* at very low light levels. J Phycol 22:39–48
Geider RJ, MacIntyre HL, Kana TM (1997) Dynamic model of phytoplankton growth and acclimation: responses of the balanced growth rate and the chlorophyll *a*:carbon ratio to light, nutrient-limitation and temperature. Mar Ecol Prog Ser 148:187–200
Gilbert RO (1987) Statistical methods for environmental pollution monitoring. Van Nostrand Reinhold Company, New York, NY

Gohin F, Druon JN, Lampert L (2002) A five channel chlorophyll concentration algorithm applied to SeaWiFS data processed by SeaDAS in coastal waters. Int J Remote Sens 23:1639–1661

Good S, Fiedler E, Mao C, Martin MJ and others (2020) The current configuration of the OSTIA system for operational production of foundation sea surface temperature and ice concentration analyses. Remote Sens 12:720

Gran HH, Braarud T (1935) A quantitative study of the phytoplankton in the Bay of Fundy and the Gulf of Maine (including observations on hydrography, chemistry, and turbidity). J Biol Board Can 1:279–467

Greene CA, Thirumalai K, Kearney KA, Delgado JM and others (2019) The Climate Data Toolbox for MATLAB. Geochem Geophys Geosyst 20:3774–3781

Haëntjens N, Boss E, Talley LD (2017) Revisiting ocean color algorithms for chlorophyll *a* and particulate organic carbon in the Southern Ocean using biogeochemical floats. J Geophys Res Oceans 122:6583–6593

Hague M, Vichi M (2021) Southern Ocean Biogeochemical Argo detect under-ice phytoplankton growth before sea ice retreat. Biogeosciences 18:25–38

Henley SF, Schofield OM, Hendry KR, Schloss IR and others (2019) Variability and change in the west Antarctic Peninsula marine system: research priorities and opportunities. Prog Oceanogr 173:208–237

Henley SF, Cavan EL, Fawcett SE, Kerr R and others (2020) Changing biogeochemistry of the Southern Ocean and its ecosystem implications. Front Mar Sci 7:581

Henson S, Cole H, Beaulieu C, Yool A (2013) The impact of global warming on seasonality of ocean primary production. Biogeosciences 10:4357–4369

Henson SA, Cole HS, Hopkins J, Martin AP, Yool A (2018) Detection of climate change-driven trends in phytoplankton phenology. Glob Change Biol 24:e101–e111

Holm-Hansen O, Hewes CD (2004) Deep chlorophyll-*a* maxima (DCMs) in Antarctic waters: I. Relationships between DCMs and the physical, chemical, and optical conditions in the upper water column. Polar Biol 27:699–710

Hu C, Lee Z, Franz B (2012) Chlorophyll *a* algorithms for oligotrophic oceans: a novel approach based on three-band reflectance difference. J Geophys Res 117:C01011

IOCCG (International Ocean Colour Coordinating Group) (2015) Ocean colour remote sensing in polar seas. In: Babin M, Arrigo K, Belanger S, Forget MH (eds) IOCCG Rep Ser 16. IOCCG, Dartmouth

IPCC (International Panel on Climate Change) (2019) IPCC special report on the ocean and cryosphere in a changing climate. Pörtner HO, Roberts DC, Masson-Delmotte V, Zhai P and others (eds). Cambridge University Press, Cambridge

Jeandel C, Ruiz-Pino D, Gjata E, Poisson A and others (1998) KERFIX, a time-series station in the Southern Ocean: a presentation. J Mar Syst 17:555–569

Joy-Warren HL, van Dijken GL, Alderkamp AC, Leventer A and others (2019) Light is the primary driver of early season phytoplankton production along the western Antarctic Peninsula. J Geophys Res Oceans 124:7375–7399

Joyce KE, Duce S, Leahy SM, Leon J, Maier SW (2019) Principles and practice of acquiring drone-based image data in marine environments. Mar Freshw Res 70:952–963

Kahru M, Mitchell BG (2010) Blending of ocean colour algorithms applied to the Southern Ocean. Remote Sens Lett 1:119–124

Kauko HM, Hattermann T, Ryan-Keogh T, Singh A and others (2021) Phenology and environmental control of phytoplankton blooms in the Kong Håkon VII Hav in the Southern Ocean. Front Mar Sci 8:623856

Kendall MG (1975) Rank correlation methods. Griffin, London

Killick R, Fearnhead P, Eckley IA (2012) Optimal detection of changepoints with a linear computational cost. J Am Stat Assoc 107:1590–1598

Kim HH, Ducklow HW, Abele D, Barlett EMR and others (2018) Inter-decadal variability of phytoplankton biomass along the coastal West Antarctic Peninsula. Philos Trans R Soc A 376:20170174

Kim HH, Luo YW, Ducklow H, Schofield O, Steinberg D, Doney S (2021) WAP-1D-VAR v1.0: development and evaluation of a one-dimensional variational data assimilation model for the marine ecosystem along the West Antarctic Peninsula. Geosci Model Dev 14:4939–4975

Kirchgäßner A (2010) An analysis of cloud observations from Vernadsky, Antarctica. Int J Climatol 30:1431–1439

Kirchgäßner A (2011) An analysis of precipitation data from the Antarctic base Faraday/Vernadsky. Int J Climatol 31: 404–414

Landschützer P, Gruber N, Haumann FA, Rödenbeck C and others (2015) The reinvigoration of the Southern Ocean carbon sink. Science 349:1221–1224

Mann HB (1945) Nonparametric tests against trend. Econometrica 13:245–259

Martinson DG (2012) Antarctic circumpolar current's role in the Antarctic ice system: an overview. Palaeogeogr Palaeoclimatol Palaeoecol 335–336:71–74

Meredith MP, Stammerjohn SE, Venables HJ, Ducklow HW and others (2017) Changing distributions of sea ice melt and meteoric water west of the Antarctic Peninsula. Deep Sea Res II 139:40–57

Meredith MP, Stammerjohn SE, Ducklow HW, Leng MJ and others (2021) Local- and large-scale drivers of variability in the coastal freshwater budget of the Western Antarctic Peninsula. J Geophys Res Oceans 126:e2021JC017172

Mitchell BG (1992) Predictive bio-optical relationships for polar oceans and marginal ice zones. J Mar Syst 3:91–105

Mitchell BG, Holm-Hansen O (1991) Bio-optical properties of Antarctic Peninsula waters: differentiation from temperate ocean models. Deep Sea Res A 38:1009–1028

Moline MA (1998) Photoadaptive response during the development of a coastal Antarctic diatom bloom and relationship to water column stability. Limnol Oceanogr 43: 146–153

Montes-Hugo M, Doney SC, Ducklow HW, Fraser W, Martinson D, Stammerjohn SE, Schofield O (2009) Recent changes in phytoplankton communities associated with rapid regional climate change along the Western Antarctic Peninsula. Science 323:1470–1473

Munro DR, Lovenduski NS, Stephens BB, Newberger T and others (2015a) Estimates of net community production in the Southern Ocean determined from time series observations (2002–2011) of nutrients, dissolved inorganic carbon, and surface ocean pCO_2 in Drake Passage. Deep Sea Res II 114:49–63

Munro DR, Lovenduski NS, Takahashi T, Stephens BB, Newberger T, Sweeney C (2015b) Recent evidence for a strengthening CO_2 sink in the Southern Ocean from carbonate system measurements in the Drake Passage (2002–2015). Geophys Res Lett 42:7623–7630

Nardelli SC, Gray PC, Stammerjohn SE, Schofield O (2023) Characterizing coastal phytoplankton seasonal succession patterns on the West Antarctic Peninsula. Limnol Oceanogr 68:845–861

Norman L, Thomas DN, Stedmon CA, Granskog MA and others (2011) The characteristics of dissolved organic matter (DOM) and chromophoric dissolved organic matter (CDOM) in Antarctic sea ice. Deep Sea Res II 58: 1075–1091

Orsi AH, Whitworth T III, Nowlin WD Jr (1995) On the meridional extent and fronts of the Antarctic Circumpolar Current. Deep Sea Res I 42:641–673

Pan BJ, Vernet M, Reynolds RA, Mitchell GB (2019) The optical and biological properties of glacial meltwater in an Antarctic fjord. PLOS ONE 14:e0211107

Patterson KW (2000) Contribution of chromophoric dissolved organic matter to attenuation of ultraviolet radiation in three contrasting coastal areas. PhD dissertation, University of California Santa Barbara, CA

Pinkerton MH, Boyd PW, Deppeler S, Hayward A, Höfer J, Moreau S (2021) Evidence for the impact of climate change on primary producers in the Southern Ocean. Front Ecol Evol 9:592027

Poloczanska ES, Brown CJ, Sydeman WJ, Kiessling W and others (2013) Global imprint of climate change on marine life. Nat Clim Change 3:919–925

Poloczanska ES, Burrows MT, Brown CJ, García Molinos J and others (2016) Responses of marine organisms to climate change across oceans. Front Mar Sci 3:62

Racault MF, Le Quéré C, Buitenhuis E, Sathyendranath S, Platt T (2012) Phytoplankton phenology in the global ocean. Ecol Indic 14:152–163

Racault MF, Raitsos DE, Berumen ML, Brewin RJW, Platt T, Sathyendranath S, Hoteit I (2015) Phytoplankton phenology indices in coral reef ecosystems: application to ocean-color observations in the Red Sea. Remote Sens Environ 160:222–234

Riley GA (1942) The relationship of vertical turbulence and spring diatom flowerings. J Mar Res 5:67–87

Saba GK, Fraser WR, Saba VS, Iannuzzi RA and others (2014) Winter and spring controls on the summer food web of the coastal West Antarctic Peninsula. Nat Commun 5: 4318

Sato K, Simmonds I (2021) Antarctic skin temperature warming related to enhanced downward longwave radiation associated with increased atmospheric advection of moisture and temperature. Environ Res Lett 16:064059

Schofield O, Brown M, Kohut J, Nardelli S, Saba G, Waite N, Ducklow H (2018) Changes in the upper ocean mixed layer and phytoplankton productivity along the West Antarctic Peninsula. Philos Trans R Soc A 376:20170173

Siegel DA, Doney SC, Yoder JA (2002) The North Atlantic spring phytoplankton bloom and Sverdrup's critical depth hypothesis. Science 296:730–733

Smith RC, Dierssen HM, Vernet M (1996) Phytoplankton biomass and productivity in the western Antarctic Peninsula region. In: Ross RM, Hofmann EE, Quetin LB (eds) Foundations for ecological research west of the Antarctic Peninsula. Antarctic Research Series. American Geophysical Union, Washington, DC, p 333–356

Stabeno PJ, Bond NA, Kachel NB, Salo SA, Schumacher JD (2001) On the temporal variability of the physical environment over the south-eastern Bering Sea. Fish Oceanogr 10:81–98

Stabeno PJ, Kachel NB, Moore SE, Napp JM, Sigler M, Yamaguchi A, Zerbini AN (2012) Comparison of warm and cold years on the southeastern Bering Sea shelf and some implications for the ecosystem. Deep Sea Res II 65-70:31–45

Stammerjohn SE, Drinkwater MR, Smith RC, Liu X (2003) Ice-atmosphere interactions during sea-ice advance and retreat in the western Antarctic Peninsula region. J Geophys Res 108:3329

Stammerjohn SE, Martinson DG, Smith RC, Yuan X, Rind D (2008) Trends in Antarctic annual sea ice retreat and advance and their relation to El Niño-Southern Oscillation and Southern Annular Mode variability. J Geophys Res 113:C03S90

Stroeve JC, Jenouvrier S, Campbell GG, Barbraud C, Delord K (2016) Mapping and assessing variability in the Antarctic marginal ice zone, pack ice and coastal polynyas in two sea ice algorithms with implications on breeding success of snow petrels. Cryosphere 10:1823–1843

Sverdrup HU (1953) On conditions for the vernal blooming of phytoplankton. ICES J Mar Sci 18:287–295

The MathWorks Inc (2019) MATLAB version: 9.6.0 (R2019a). The MathWorks Inc., Natick, MA. https://www.mathworks.com

Thibodeau PS, Steinberg DK, Stammerjohn SE, Hauri C (2019) Environmental controls on pteropod biogeography along the Western Antarctic Peninsula. Limnol Oceanogr 64:S240–S256

Thomalla SJ, Racault MF, Swart S, Monteiro PMS (2015) High-resolution view of the spring bloom initiation and net community production in the Subantarctic Southern Ocean using glider data. ICES J Mar Sci 72:1999–2020

Tréguer P, Jacques G (1992) Dynamics of nutrients and phytoplankton, and fluxes of carbon, nitrogen and silicon in the Antarctic Ocean. Polar Biol 12:149–162

Turner JS (2024) A data repository for: Changing phytoplankton phenology in the marginal ice zone west of the Antarctic Peninsula. Zenodo. https://doi.org/10.5281/zenodo.10790613

Turner J, Maksym T, Phillips T, Marshall GJ, Meredith MP (2013) The impact of changes in sea ice advance on the large winter warming on the western Antarctic Peninsula. Int J Climatol 33:852–861

van Leeuwe MA, Webb AL, Venables HJ, Visser RJW, Meredith MP, Elzenga JTM, Stefels J (2020) Annual patterns in phytoplankton phenology in Antarctic coastal waters explained by environmental drivers. Limnol Oceanogr 65:1651–1668

Van Oostende M, Hieronymi M, Krasemann H, Baschek B, Röttgers R (2022) Correction of inter-mission inconsistencies in merged ocean colour satellite data. Front Remote Sens 3:882418

Venables HJ, Clarke A, Meredith MP (2013) Wintertime controls on summer stratification and productivity at the western Antarctic Peninsula. Limnol Oceanogr 58:1035–1047

Vernet M, Martinson D, Iannuzzi R, Stammerjohn S and others (2008) Primary production within the sea-ice zone west of the Antarctic Peninsula: I–Sea ice, summer mixed layer, and irradiance. Deep Sea Res II 55:2068–2085

Vichi M (2022) An indicator of sea ice variability for the Antarctic marginal ice zone. Cryosphere 16:4087–4106

Vives CR, Schallenberg C, Strutton PG, Boyd PW (2023) Biogeochemical-Argo floats show that chlorophyll increases before carbon in the high-latitude Southern Ocean spring bloom. Limnol Oceanogr Lett (in press) doi:10.1002/lol2.10322

Weinstein BG, Friedlaender AS (2017) Dynamic foraging of a top predator in a seasonal polar marine environment. Oecologia 185:427–435

Winder M, Sommer U (2012) Phytoplankton response to a

changing climate. Hydrobiologia 698:5–16
Xue L, Gao L, Cai W, Yu W, Wei M (2015) Response of sea surface fugacity of CO_2 to the SAM shift south of Tasmania: regional differences. Geophys Res Lett 42:3973–3979
Yu L, Zhong S, Sun B (2020) The climatology and trend of surface wind speed over Antarctica and the Southern Ocean and the implication to wind energy application. Atmosphere 11:108

Appendix. Definitions used

Term or abbreviation	Definition
Accumulation season	Period each year when surface chlorophyll *a* (chl *a*) concentration is increasing such that average phytoplankton mass-specific loss rates < growth rates
Chl *a*	Chlorophyll *a* concentration (mg m^{-3})
CMEMS	Copernicus Marine Environmental Monitoring Service
CZCS	Coastal Zone Color Scanner sensor
ERA5	ECMWF Re-Analysis Version 5, a climate reanalysis data product generated by the European Centre for Medium-Range Weather Forecasts (ECMFW).
MERIS	Medium Resolution Imaging Spectrometer sensor
MIZ	Marginal ice zone
MLD	Mixed-layer depth
MODIS-Aqua	Moderate Resolution Imaging Spectroradiometer sensor on the Aqua satellite
MODIS-Terra	Moderate Resolution Imaging Spectroradiometer sensor on the Terra satellite
OLCI-S3A	Ocean and Land Colour Instrument sensor on the Sentinel-3A satellite
OLCI-S3B	Ocean and Land Colour Instrument sensor on the Sentinel-3B satellite
OSTIA	Operational Sea Surface Temperature and Sea Ice Analysis
PAR	Photosynthetically active radiation
pCO_2	Partial pressure of carbon dioxide
Peak date	Day of year of the timing of the maximum chl *a* concentration
SAM	Southern Annular Mode
SeaWiFS	Sea-viewing Wide Field-of-view Sensor
SPF	Southern Polar Front
SST	Sea surface temperature
Start date	Day of year of the start of the phytoplankton accumulation season
Threshold	Value defining bloom start date; long-term median chl *a* + 5%
VIIRS-NOAA20	Visible Infrared Imaging Radiometer Suite sensor on the NOAA-20 satellite
VIIRS-NPP	Visible Infrared Imaging Radiometer Suite sensor on the National Polar-orbiting Partnership satellite
WAP	West Antarctic Peninsula

Editorial responsibility: Antonio Bode, A Coruña, Spain
Reviewed by: M. Pinkerton and 1 anonymous referee

Submitted: November 1, 2023
Accepted: February 27, 2024
Proofs received from author(s): April 13, 2024